arXiv:1210.0021v1 [hep-ex] 28 Sep 2012

Searches for the Standard Model Higgs Boson at Hadron Colliders at $\sqrt{s} = 2$, 7 and 8 TeV until the Discovery of the $\simeq 125$ GeV Boson

Gregorio Bernardi[1] and Matthew Herndon[2]

[1]*LPNHE, Universités Paris VI & VII, CNRS/IN2P3, Paris, France*
[2]*University of Wisconsin, Madison, Wisconsin, USA*

We review the experimental searches for the standard model (SM) Higgs boson at the 2 TeV Run of the Tevatron with $\simeq 10$ fb^{-1} of recorded data, and at the 7 and 8 TeV Runs of the LHC, with $\simeq 5$ and $\simeq 6$ fb^{-1} respectively. The CMS and ATLAS collaborations observe independently a new particle with mass $\simeq 125$ GeV, mainly through its bosonic decays in $\gamma\gamma$, ZZ, and WW, consistent with the SM Higgs boson. The CDF and D0 experiments combine their result to see evidence of a similar particle produced in association with a vector boson and decaying fermionically, in $b\bar{b}$.

PACS numbers: 13.85.Rm, 14.80.Bn

Contents

I. Introduction 2

II. SM Higgs phenomenology and search strategies 2
- A. phenomenology of SM Higgs production 2
- B. phenomenology of SM Higgs decay 3
- C. Standard model fits 3
- D. Direct constraints from LEP 3
- E. Search strategies at the Tevatron 4
- F. Search strategies at the LHC 4
- G. Simulation of background and signal processes 4

III. Tevatron Experiments 5
- A. The Tevatron and the CDF and D0 detectors 5
  - 1. Tracking Detectors 5
  - 2. Calorimeters 5
  - 3. Muon Detectors 5
  - 4. Triggering systems 6
  - 5. lepton identification 6
  - 6. Jets, b-jets, and Missing Transverse energy 6

IV. Tevatron Low mass Higgs searches 7
- A. VZ with $Z \to b\bar{b}$ as test of the VH search 7
- B. $WH \to l\nu b\bar{b}$ 7
- C. $ZH \to llb\bar{b}$ 8
- D. $ZH \to \nu\nu b\bar{b}/VH \to \not\!\!E_T b\bar{b}$ 9
- E. CDF and D0 results on $H \to b\bar{b}$ searches 9
- F. Searches with τ_h in the final state 10
- G. Searches for $H \to \gamma\gamma$ 10
- H. Searches for $t\bar{t}H$ production 10

V. Tevatron High mass Higgs searches 10
- A. Diboson analysis: WW, WZ and ZZ 11
- B. Analysis Topologies 11
- C. CDF and D0 results at high Higgs mass 13

VI. LHC Experiments 13
- A. The LHC and the ATLAS and CMS experiments 13
  - 1. Tracking Detectors 14
  - 2. Calorimeters 14
  - 3. Muons systems 14
  - 4. Particle flow 15
  - 5. Triggering 15
- B. Physics object identification at the LHC 15
  - 1. Charged Lepton Identification 15
  - 2. Photon Identification 16
  - 3. Light and Heavy Flavor Jets 16
  - 4. Missing Transverse Energy 16
- C. Higgs Production and Decay at the LHC 16
- D. LHC Diboson Physics 17

VII. LHC searches in fermionic Higgs decays 17
- A. Searches for $t\bar{t}H$ production 17
- B. Higgs searches with $H \to bb$ 17
- C. Higgs searches with $H \to \tau^+\tau^-$ 18

VIII. LHC searches in bosonic Higgs decays 18
- A. Higgs searches with $H \to WW, ZZ$ with decays of one boson to quarks or neutrinos 18
- B. Higgs searches with $H \to W^+W^- \to \ell^+\nu\ell^-\bar{\nu}$ 19
- C. Higgs searches with $H \to ZZ \to \ell^+\ell^-\ell^+\ell^-$ 19
- D. Higgs searches with $H \to \gamma\gamma$ 21

IX. Tevatron, ATLAS, and CMS Results 22
- A. Limits and Combination methods 22
- B. Tevatron combined results 22
- C. ATLAS and CMS combined results 25
- D. Conclusion and Prospects 30

References 30

I. INTRODUCTION

Among the puzzles of such a successful theory as the Standard Model (SM), the origin of the mass of the elementary particles has a potential solution. With the adjunction of only one doublet of complex scalar fields, the finite mass of the SM elementary fermions and bosons can be explained, after spontaneous electroweak symmetry breaking (EWSB) of the originally massless Lagrangian [1, 2]. This minimal approach could be confirmed if the remnant of such a breaking, the Higgs boson, is observed with the couplings and properties predicted in the SM. The SM Higgs boson does not solve all problems related to the EWSB, and is maybe only one component of the fields involved. However, its discovery would be a major step in the final validation of the Standard Model in that it would show a unified approach to the mass generation, hence its crucial importance. While there are other approaches to explain EWSB, none is so far as successful as the Higgs mechanism, so we concentrate in this review on the experimental searches for such a boson. With the recent observation of a new boson at the LHC, a major step forward has been accomplished, but a complete validation has yet to be done. The data taking has been concluded at the Tevatron and at the LHC for the center of mass energy of 7 TeV, while the data are still being accumulated at 8 TeV. However, given the recent discovery in these searches, we provide a dedicated review based on the publications which immediately followed the discovery.

To review these milestone results, we first briefly explain the phenomenology of the production and decay of the SM Higgs boson, the indirect constraints on the SM Higgs from other measurements, and the search strategies at the Tevatron and the LHC. Then we review the Tevatron experiments, and their low mass and high mass analyses. Next we review the LHC experiments, and their searches in fermionic and bosonic Higgs boson decays. Finally we review the combinations of these searches, first from the Tevatron, then from ATLAS and CMS, before concluding briefly on the current knowledge on this new boson, and on short term prospects.

II. SM HIGGS PHENOMENOLOGY AND SEARCH STRATEGIES

A. phenomenology of SM Higgs production

The SM Higgs boson is a CP-even scalar, and its couplings to fermions and to gauge bosons are proportional to the fermion masses, and to the squares of the boson masses, respectively. The effective Higgs-gluons coupling, Hgg, is dominated at leading order by a one-loop graph in which the H couples to a virtual $t\bar{t}$ pair. The much weaker effective coupling to photons, $H\gamma\gamma$, proceeds also at LO via a loop, dominated by a virtual WW pair [3]. The dominant cross section for Higgs production is the $gg \to H$ process, which is known at next-to-next-to-leading order (NNLO) in QCD, in the large top-mass limit, and at NLO in QCD for arbitrary top mass [4]. The NLO QCD corrections approximately double the leading-order prediction, and the NNLO corrections add approximately 50% to the NLO prediction. NLO electroweak corrections range between 0 and 6% of the LO term [5]. Mixed QCD-electroweak In addition, soft-gluon contributions to the cross sections have been resumed at next-to-leading logarithmic (NLL), NNLL and partial NNNLL accuracy [7]. Updated predictions for the gluon fusion cross sections at NNLO or through soft-gluon resummation up to next-to-next-to-leading logarithmic accuracy (NNLL), and two-loop electroweak effects can be found in Ref. [6, 8–10], including differential distributions vs. transverse momentum [11, 12]. Uncertainties are dominated by PDF and scale choices and are $\simeq$ 25% at the Tevatron and $\simeq$ 15% at the LHC. These cross sections have also been computed exclusively, for Higgs boson production in association with one, two, or more jets [13].

At the Tevatron, the next most important production processes are Higgs boson production in association with vector bosons. These cross sections $q\bar{q} \to WH$ or ZH are known at NNLO for the QCD corrections and at NLO for the electroweak corrections [14, 15], with a total uncertainty of $\simeq$ 5%. For the vector boson fusion processes $qq \to qqH$, which dominates over the associated production at the LHC, the production cross sections are known at NNLO in QCD and at NLO for the electroweak corrections, with a small total theoretical uncertainty, $\simeq$ 5% [16], which becomes larger when exclusive conditions are put on the jets [17]. For the associated production process $t\bar{t}H$, the cross section has been calculated at NLO in QCD [18].

The cross sections for the production of SM Higgs bosons are summarized in figure 1 for $p\bar{p}$ collisions at the Tevatron, and in figure 2 for pp collisions at the LHC, at

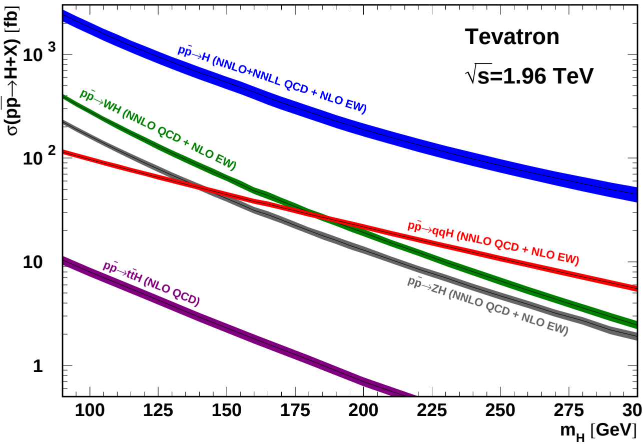

FIG. 1: SM Higgs boson production cross sections for $p\overline{p}$ collisions at 1.96 TeV [4, 15, 16, 18], as functions of its mass.

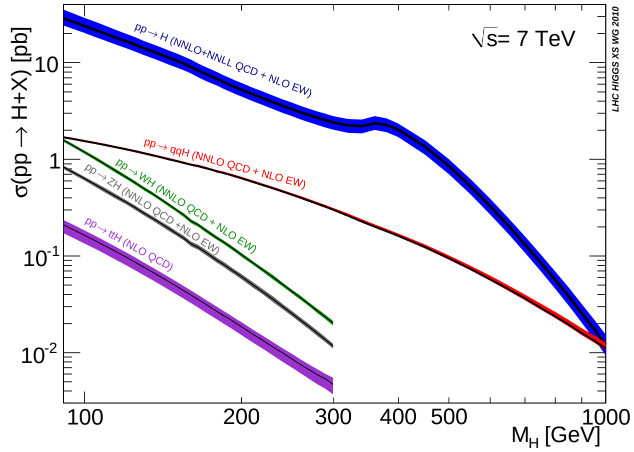

FIG. 2: SM Higgs boson production cross sections for pp collisions at 7 TeV [19], as functions of its mass.

$\sqrt{s} = 7$ TeV [19, 20]. Cross sections at $\sqrt{s} = 8$ TeV have a similar behvior but 20-30% larger at low Higgs mass.

B. phenomenology of SM Higgs decay

The branching ratios for the most relevant decay modes of the SM Higgs boson are shown in figure 3 as functions of m_H. For masses below 135 GeV, decays to fermion pairs dominate, of which the decay $H \to b\bar{b}$ has the largest branching ratio. For these low masses, the total decay width is less than 10 MeV. For Higgs boson masses above 135 GeV, the WW decay dominates with an important contribution from $H \to ZZ$ above threshold. The decay width rises rapidly, reaching about 1 GeV at $m_H = 200$ GeV and 100 GeV at $m_H = 500$ GeV. Above the $t\bar{t}$ threshold, the branching ratio into top-quark pairs increases rapidly as a function of the Higgs boson mass, reaching a maximum of about 20% at $m_H \simeq 450$ GeV.

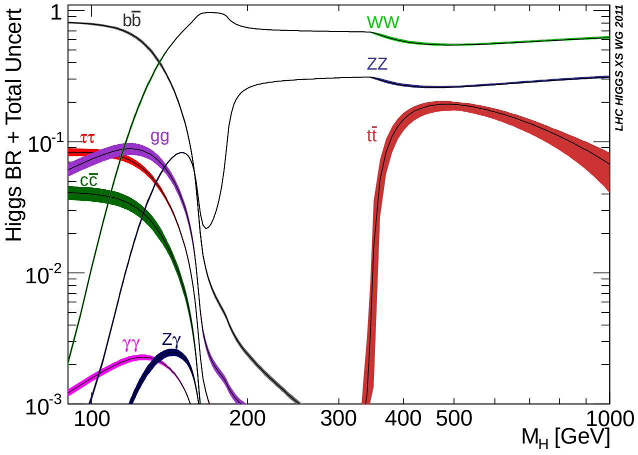

FIG. 3: Branching ratios for the main decays of the SM Higgs boson as functions of its mass

C. Standard model fits

While the mass of the SM Higgs boson is not given by the theory, indirect constraints for the SM Higgs boson mass can be derived from fits to precision measurements of electroweak observables. The Higgs boson contributes to the W and Z vacuum polarization through loop effects, leading to a logarithmic sensitivity of the ratio of the W and Z gauge boson masses on the Higgs boson mass. The top quark contributes to the W boson vacuum polarization through loop effects that depend quadratically on the top mass, which thus also plays an important role in the global fit. A global fit to precision electroweak data, accumulated in the last two decades mainly at LEP, SLC, the Tevatron, gives $m_H = 94^{+29}_{-24}$ GeV, or $m_H < 152$ GeV at 95% C.L. [21]. Measurements of the top quark mass (173.2 ± 0.9 GeV [22]) and of the W boson mass (80.385 ± 0.015 GeV [23]) were used for these constraints. These results, compared to the allowed direct search range from March 2012 are shown in figure 4.

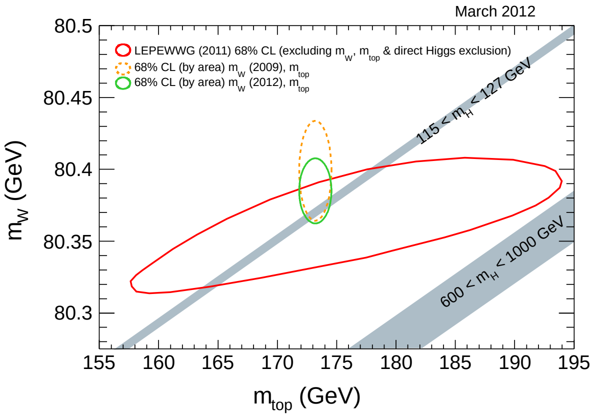

FIG. 4: Constraints given by top, W and other SM measurements compared to the allowed Higgs search range in March 2012.

D. Direct constraints from LEP

At the LEP e^+e^- collider, which operated between 1989 and 2000 at $\sqrt{s} = 90$ GeV (LEP1) or 160-209 GeV (LEP2), the SM Higgs boson is generally produced through Higgsstrahlung in the s-channel,$e^+e^- \to HZ$ [24, 25], where the Z boson in the final state is either virtual (LEP1), or on mass shell (LEP2). The SM Higgs boson can also be produced by WW and ZZ fusion in the t-channel [26], but at LEP these processes have small cross sections. The sensitivity of the LEP searches to the Higgs boson strongly depends on the center-of-mass energy, E_{CM}. For $m_H < E_{\mathrm{CM}} - m_Z$, the cross section is of order 1 pb or more, while for $m_H > E_{\mathrm{CM}} - m_Z$, the cross section is smaller by at least an order of magnitude.

Each production and decay mode was analyzed separately. Data recorded at each center-of-mass energy were studied independently and the results from the four LEP experiments were then combined. Strong upper bounds on the $e^+e^- \to ZH$ cross section are obtained for Higgs masses between 1 KeV and $\simeq$ 115 GeV. The combination of the LEP data yields a 95% C.L. lower bound of 114.4 GeV for the mass of the SM Higgs boson [27]. The median limit expected in a large ensemble of identical experiments when no signal is present (simply called "expected limit" in the following) is 115.3 GeV, and was constrained by the collision energy achieved by the accelerator.

E. Search strategies at the Tevatron

At the Tevatron, the delivered luminosity and the Higgs production cross section are sufficient to be sensitive at the 95% CL to a Higgs boson having a mass between 90 GeV and 190 GeV, i.e. significant overlap with the LEP excluded region at low mass, and with the LHC at higher mass. Sensitivity is strongest at low mass, 115-125 GeV (not considering the excluded LEP region) and at the $H \to WW$ threshold ($\simeq$ 160 GeV) where the expected sensitivity reaches approximately 4 standard deviations.

The search strategy gives priority to direct production and $H \to WW$ decay mode at high mass, which allowed in 2009 to extend the LEP exclusion limit for the first time after almost ten years [28]. This result in combination with the precision electroweak measurements showed, before the LHC produced significant results, that a mass of the SM Higgs boson above $\simeq$ 145 GeV was excluded at 95%CL [29]

At low mass, the associated production channels (WH, ZH) involving $H \to b\bar{b}$ are the most sensitive, with significant contribution from direct production $H \to WW$ down to 120 GeV. The WH and ZH channels with $H \to b\bar{b}$ are particularly important since this decay mode will not be measured precisely at the LHC before the upgrade to the full energy foreseen for 2015.

F. Search strategies at the LHC

The LHC was designed to have a full reach to discover the Higgs boson, from 0.1 to 1 TeV, which is the region where it was theoretically expected to be. The low masses, below approximately 140 GeV, are more difficult, since the lowest background channel in which the Higgs boson decays in a pair of Z bosons, has low branching ratio, and at least one of the Z is not on-shell. In this region, the low branching ratio decay channel in a pair of photons is most efficient. Both modes allow possible discovery as soon as the available integrated luminosity is sufficient (of the order of 10 fb^{-1}). No single channel dominates the sensitivity, so the search is also performed through combination of all channels.

Because of a more unfavorable signal to background ratio in associated production (due to the initial dominant qq or gg vs. $q\bar{q}$ hard interaction), the search strategy gives priority to direct production and $H \to \gamma\gamma$ or $H \to ZZ$ decay mode at low mass, or simply to $H \to ZZ$ at higher masses. The $H \to WW$ channel has also good sensitivity and is necessary to search in the region around the WW on shell decay threshold, but does not have the mass resolution to observe a clear resonance signal.

However, once a new particle is observed all channels are crucial to understand its nature. In particular the fermionic decays (in pairs of τ leptons or b quarks) are a major source of information on fermion couplings, but require a higher luminosity. Other fermionic decays are not observable in a foreseeable future, assuming standard model branching ratios, though information is gained about the Higgs coupling to the top quark through the loop production diagrams.

G. Simulation of background and signal processes

The general strategies used to generate background and signal processes at both the Tevatron and LHC are summarized in this section.

i) High cross section backgrounds W/Z + jets, diboson: the SM background processes $Wq\bar{q} \to \ell\nu q\bar{q}$ or $Zq\bar{q} \to \ell^+\ell^- q\bar{q}$, where q is used to represent light partons u, d, s and gluons (g), and higher cross section diboson processes, are simulated using the Monte Carlo (MC) matrix element event generators such as `ALPGEN, MADGRAPH and POWHEG`. Separate samples are generated for light parton multiplicities and in each case samples are generated for each of the final state decay lepton flavors $\ell = e, \mu, \tau$. To account for the subsequent hadronization and development of partonic showers the matrix event generators are interfaced to `PYTHIA` according to the MLM factorization ("matching") scheme.

ii) top, single top and diboson production: $t\bar{t}$ production has been studied since the Tevatron Run 1 and is now also studied at the LHC. The electroweak production of (single) top-quark has been observed at the Tevatron by the CDF and D0 collaboration in 2008 [30, 31] and also by the LHC experiments. Similarly diboson production $(WW/WZ/ZZ)$ have been measured at the Tevatron and LHC. Extensive studies of top, single top, and diboson production have been performed by the collaborations showing that the normalization and kinematic distributions of these process are well modeled by a variety of programs including `CompHep,MC@NLO,MADGRAPH,POWHEG` interfaced to `PYTHIA`. In cases where there are multiple additional partons in the final state, the data are not as constraining and the techniques listed in section i) are applied.

iii) b-tagged backgrounds, $Wb\bar{b}$, $Zb\bar{b}$, single top, tW, and $t\bar{t}$ production: These production processes are generated using similar techniques to those described above. However, substantial scale factors to account for efficiency differences in simulation and data for b-jet tagging are applied and in the case of associated vector boson with heavy flavor production normalization k-factors measured in the data are applied as the total cross sections are not well predicted.

iv) The diboson processes WW and ZZ also have substantial contributions from gluon-gluon initial states which are generated using the specialized generators `GG2WW` and `GG2ZZ`.

Signal samples are generated using programs such as `PYTHIA` and `POWHEG` interfaced to `PYTHIA`. In the case of gluon fusion production the kinematics understood at NNLO can differ from leading order generation and samples are re-weighed to differential NNLO calculations.

For each background or signal the total cross section is normalized to the best available NLO or NNLO calculations.

III. TEVATRON EXPERIMENTS

A. The Tevatron and the CDF and D0 detectors

The Tevatron is a proton-antiproton collider. The Higgs searches took place during Run II (2002-2012) in which it was configured to collide beams of 36 bunches with 1.96 TeV center of mass energy and provided an integrated dataset of 10 fb^{-1} to the CDF and D0 experiments. The instantaneous luminosity reached 4.10^{32} cm^2 s^{-1} but the effect of the overlay of multiple interactions remained manageable.

The main components of the Run II CDF and D0 detectors are the tracking detectors, calorimeters and muon detectors. Specific details of the CDF and D0 detector subsystems are available in [32] and [33] respectively, while here below we briefly summarize their main characteristics. The kinematic properties of particles and jets are defined with respect to the origin of the detector coordinate system which is at the center of the detector. To quantify polar angles the pseudorapidity variable, defined as $\eta = -\ln\tan\frac{\theta}{2}$, is used where θ is the polar angle in the corresponding spherical polar coordinate system.

1. *Tracking Detectors*

The CDF tracking system consists of an eight layer silicon micro-strip tracker and an open-cell drift chamber referred to as the Central Outer Tracker (COT), both immersed in a 1.4 T solenoidal magnetic field. These systems combined provide charged particle tracking and precision vertex reconstruction in the pseudorapidity region $|\eta| < 1.0$ and partial coverage in the COT to $|\eta| < 1.7$ while the outer two layers of the silicon detector include forward elements that extend the tracking capability to $|\eta| < 2.0$.

The D0 tracking system is located immediately surrounding the interaction point and consists of an inner silicon micro-strip tracker (SMT) surrounded by an outer central scintillating fiber tracker (CFT). Both the SMT and CFT are situated within a 2 T magnetic field provided by a solenoidal magnet surrounding the entire tracking system. The SMT is used for tracking up to $|\eta| = 2.5$ and for vertex reconstruction. The central fiber tracker is also used for vertex reconstruction, and provides precise tracking coverage up to $|\eta| = 1.7$.

2. *Calorimeters*

The CDF Calorimeter systems are used to measure the energy both charged and neutral particles produced $p\bar{p}$ collisions and are arranged around the outer edges of the central tracking volume and solenoid. These systems consist of modular sampling scintillator calorimeters with a tower based projective geometry. The inner electromagnetic sections of each tower consist of lead sheets interspersed with scintillator, and the outer hadronic sections are composed of scintillator sandwiched between sheets of steel. The CDF calorimeter consists of two sections: a central barrel calorimeter and forward end plug calorimeters covering the pseudorapidity region $|eta| < 3.64$. The calorimeters can identify and measure photons, jets from partons, missing transverse energy, and in combination with other systems electrons and tau leptons.

The D0 liquid argon calorimeter system is used for energy measurement and identification of electrons, photons, and jets, and also allows to measure the missing transverse energy ($\not{E}_T$) of the events. The central calorimeter (CC) covers detector pseudorapidities $|\eta| \leq 1.1$ and the two additional end-cap calorimeters (EC) extend the range up to $|\eta| = 4.2$. They are located outside of the tracking and solenoid systems. The calorimeters are subdivided into electromagnetic (EM) followed by fine hadronic and then coarse hadronic sections. The inter-cryostat (ICR) plastic scintillator detectors complete the calorimeter coverage in the intermediate pseudorapidity region $0.8 < |\eta| < 1.4$.

3. *Muon Detectors*

The CDF muon detector is made up of four independent detector systems outside the calorimeter modules and consists of drift chambers interspersed with steel layers to absorb hadrons. The Central Muon Detector (CMU) is mounted directly around the outer edge of the central calorimeter module an detects muons in the pseudorapidity region $|\eta| < 0.6$. The central muon extension is composed on spherical sections and extends the pseudorapidity coverage from $0.6 < |\eta| < 1.0$. The CMP surrounds portions of the CMU and CMX systems covering gaps in angular coverage and allowing pure identification of higher momentum muons due to additional layers of steel absorber. The barrel muon upgrade (BMU) extends is a barrel shaped extension of the muon system in the pseudorapidity region from $1.0 < |\eta| < 1.5$. The CMX, CMP and BMU systems also include matching scintillator systems which provide timing information to help identify collision produced muons.

The D0 muon detector system consists of a central muon detector system covering the range $|\eta| < 1$ and a forward muon system which covers the region $1 < |\eta| < 2$. Scintillation counters are included for triggering purposes and a 1.8 T toroidal additional magnet makes it possible to determine muon momenta and perform tracking measurements with the muon system alone, although in general the central tracking is also used for muon reconstruction.

4. Triggering systems

The CDF trigger system consists of three levels. Level one consists of dedicated hardware that operates at the beam crossing frequency The level one can identify and measure the transverse momentum of charged particles using COT information and be combined with information for the calorimeters or muons system provide a trigger for leptons. The calorimeter systems can measure energy clusters which are used find jets and photons or an imbalance in transverse energy interpreted as $\not\!\!E_T$. The second level of the CDF trigger refines the measurements of level one at higher precision. The level two trigger can also include tracking and vertexing information from the silicon detectors. The third level of the trigger operates on commercial computers (PCs) and executes fast versions of the full offline reconstruction software.

The D0 trigger system has three trigger levels referred to as L1, L2 and L3. Each consecutive level receives a lower rate of events for further examination. The L1 hardware based elements of the triggers used in the electron channel typically require calorimeter energy signatures consistent with an electrons. This is expanded to include trigger algorithms requiring an electromagnetic object together with at least one jet for which the L1 requirement is calorimeter energy depositions consistent with high p_T jets. For muon samples, events are triggered using the logical .OR. of the full list of available triggers of the D0 experiment. The muon pseudorapidity coverage is restricted to $|\eta| < 1.6$ where the majority of the W+jet events ($\simeq$65%) are collected by triggers requiring high-p_T muons at L1. Events not selected by the high-p_T muon triggers are primarily collected by jet triggers.

5. lepton identification

Isolated electrons are reconstructed in the calorimeter and are selected in the pseudorapidity regions $|\eta| < 2.8$ at CDF, and at $|\eta| < 1.1$ and $1.5 < |\eta| < 2.5$ at D0. The EM showers are required to pass spatial distribution requirements consistent with those expected from electrons for each section of the calorimeter. In the D0 CC region, a reconstructed track, isolated from other tracks, is also required to be matched to the EM shower while in CDF a track is required within the coverage of the COT tracker.

Muons are selected by requiring a local track spanning all layers of the muon detector system (for D0 both within as well as outside of the toroidal magnet). A spatial match is then required to a corresponding track in the COT (CDF) or central fiber tracker (D0). To suppress muon multijet background events originating from the semi-leptonic decay of hadrons, muon candidate tracks are required to be separated from jets by a least $\Delta R = \sqrt{(\Delta y)^2 + (\Delta\phi)^2} > 0.5$. A veto against cosmic ray muons is also applied using scintillator timing information in D0 and specialized tracking algorithm to track both sides of the comic ray muon in CDF. Muons can also be identified as minimum ionizing isolated track in CDF in regions without muon coverage.

In CDF NN multivariate algorithms to enhance efficiency and background rejection are applied in some electron and muon based analysis.

Tau lepton decays into hadrons are characterized as narrow, isolated jets with lower track multiplicity than quark or gluon jets. Three types of tau lepton decays are distinguished by their detector signature. One-prong tau decays consisting of energy deposited in the hadronic calorimeter associated with a single track are denoted as tau-type 1; tau-type 2 corresponds to one-prong tau decays with energy deposited in both the hadronic and EM calorimeters, associated with a single track; and tau-type 3 are multi-prong decays with energy in the calorimeter and two or more associated tracks with invariant mass below 1.7 GeV. In D0, A set of neural networks, one for each tau-type, is applied to discriminate hadronic tau decays from jets. The input variables are related to isolation and shower shapes, and exploit correlations between calorimeter energy deposits and tracks. When requiring the neural network discriminants (NN) to be NN > 0.9 for tau-type 1,2 and NN > 0.95 for tau-type 3, typically 65% of taus are retained, while 98% of the multijet background is rejected. In CDF BDT based algorithms are used for the same purpose.

6. Jets, b-jets, and Missing Transverse energy

In CDF, Jets are reconstructed using a calorimeter based clustering algorithm. In D0, Jets are reconstructed in the calorimeters for $|\eta| < 2.5$ using the D0 Run II iterative cone algorithm. Calorimeter energy deposits within a cone of size $\Delta R < 0.5$ are used to form the jets. Different individual cell energy thresholds are applied to clustered and isolated cells. The energy of the jets is calibrated by applying a jet energy scale correction determined using γ+jet events.

Differences in jet identification efficiency and jet resolutions are adjusted in the simulation to match those measured in data. At high instantaneous luminosity, the jets are further required to have at least two tracks with $p_T > 0.5$ GeV associated with the primary vertex at D0.

At both CDF and D0, the identification of quarks initiated by a b quark ("b-tagging") is done in two steps [34] the jets are first required to pass a taggability requirement based on charged particle tracking and vertexing information, to ensure that they originate from the interaction vertex and that they contain charged tracks. At D0 in a second step a b-tagging neural network (NN) is applied to the taggable jets. This NN uses a combination of seven input variables, five of which make use secondary vertex information; the number and mass of vertices, the number of and χ^2 of the vertex contributing tracks, and the decay length significance in the xy-plane. Two further impact parameter based variables are also used. At CDF the next step in b-tagging is done using a NN with similar variables but including additional track quality information [35]. The CDF experiment also employs a cut based secondary vertex tagger [36] As and example at D0 the typical efficiency for identifying a $p_T = 50$ GeV jet that contains a b hadron is $(59 \pm 1)\%$ at a misidentification rate of 1.5% for light parton (u, d, s, g) initiated jets. This operating point is typically used for event with two "loose" (L) b-tagged jets. When tightening (T) the identification requirement the efficiency for identifying a jet with transverse momentum p_T of 50 GeV that contains a b hadron is $(48 \pm 1)\%$ with a misidentification rate of 0.5% for light parton jets.

The event missing transverse energy ($\not\!\!E_T$)is calculated from individual calorimeter cell energies in the calorimeter. It is corrected for the presence of any muons and all energy corrections to leptons or to the jets are propagated to $\not\!\!E_T$. In addition both experiments use comparison to missing transverse momentum measured using charged tracks to identify events with false $\not\!\!E_T$. The CDF experiment employs an algorithm that combines tracking and calorimeter information to improve $\not\!\!E_T$resolution.

IV. TEVATRON LOW MASS HIGGS SEARCHES

At low mass ($m_H < 135$ GeV), the dominant decay of the Higgs boson is $H \to b\bar{b}$, and it is useless to search for direct ($gg \to H$) Higgs production in this decay mode, due to the overwhelming multijet background. However, $q\bar{q}$ annihilation produces associated vector boson-Higgs production (VH) in $p\bar{p}$ collisions with a better signal to background ratio than at a pp collider. From VH originate the "primary" channels for searching for a low mass Higgs boson at the Tevatron, i.e. WH and ZH production which are best studied in the $\ell\nu b\bar{b}$, $\ell\ell b\bar{b}$ or $\nu\nu b\bar{b}$ final states. The lower branching ratios of the other decay modes render their sensitivity smaller than these primary channels but are also searched for to provide additional sensitivity in the combination of all channels.

The associated production analyses generally proceed in three steps: a preselection step, where the boson and the jets are selected, which has high statistics, hence allowing to validate in detail the background modeling. The W and Z are required to decay leptonically (topologies where W or Z decay hadronically are also searched for, but are less sensitive [37]) to facilitate the triggering and the event selection. Electrons and muons (including those coming from taus decaying leptonically) allow for a relatively pure selection, but $Z \to \nu\nu$ decays are also exploited. In the selection step, at least one jet is required to be identified as a b-quark jet, hence enhancing the signal to noise in separate final subsamples depending on the number and type of b-quark jets found. In the final step, multivariate analysis (MVA) techniques are applied to each of the samples, to further separate the signal from the background.

Vector boson production and direct Higgs production can also be exploited when the Higgs decays in a $\tau\tau$ pair, by making use of the kinematics of the additional jets in the final state. These processes suffer from significant background and so are considered as secondary channels at the Tevatron. Another secondary channel which is exploited at the Tevatron is direct production of Higgs, followed by Higgs to two photons decay. The sensitivity of this channel is low due to the small branching ratio of this decay, typically smaller than 0.2 %. The $t\bar{t}H$ production is also searched for, but has low sensitivity.

In all the analyses, the data are separated into multiple orthogonal search samples of varying sensitivities. The analyses are described below and all results are summarized in section X.

A. VZ with $Z \to b\bar{b}$ as test of the VH search

Since the low mass analyses use advanced techniques and have low signal-to-background, a crucial test has been performed on WZ/ZZ diboson production where one Z decays to heavy flavor, hence mimicking the final state of WH/ZH together with displaying resonant dijet production. In such analyses the WW process is taken as a background, with a normalization constrained to its NLO cross section. These analyses, and their combination, are performed in the same way as their Higgs counterparts. The CDF+D0 combination displays strong evidence (4.6 σ) for such production, with a measured croass section $\sigma(VZ) = 4.47 \pm 0.97$ pb consistent with the standard model prediction [38]. Evidence was first seen by both collaborations separately [39, 40] using 9.5 and 7.5 fb^{-1} respectively.

B. $WH \to l\nu b\bar{b}$

The search for the process $q\bar{q} \to WH + X$ in which a quark-antiquark pair leads to the production of the Higgs in association with a W boson, is based on a total integrated luminosity $\mathcal{L} \simeq 10$ fb^{-1} of collision data collected by both the CDF and D0 detectors at the Fermilab Tevatron $p\bar{p}$ collider between 2002 and 2011 [41–44]. Candi-

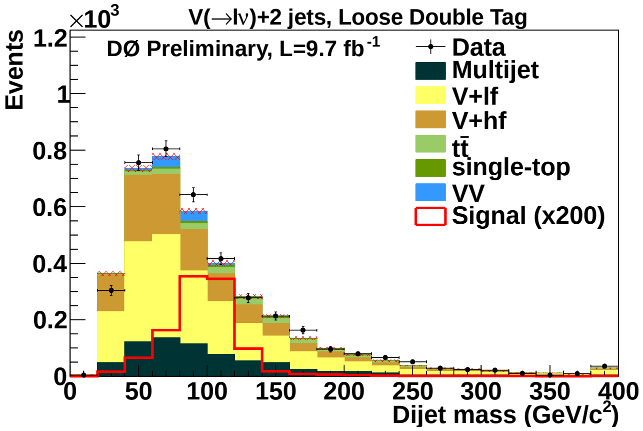

FIG. 5: Dijet mass distribution in the D0 WH analysis for the $W+2$ jet sample with 2 b-jets. The data are well described by the sum of all the standard model backgrounds. The simulated signal is also represented.

date W boson events are preselected via their decays to an electron or a muon plus a neutrino ($W \to e$ or $\mu\nu$) while the Higgs boson is searched though its decay mode into a pair of b-quarks ($H \to b\bar{b}$). The experimental signature is a single isolated lepton, missing transverse energy, and either two or three (to accomodate additional radiation of a QCD parton in the hard collision) jets, at least one of which is required to be consistent with having been initiated by a b-quark.

To increase signal acceptance, the lepton identification criteria are as loose as possible. This results into instrumental background originating from multijet (MJ) events, in which one of the jet is misidentified as an isolated lepton. In CDF, the MJ background is strongly reduced by kinematic cuts and by using a dedicated multivariate technique against such background [42]. The remaining MJ background contribution is determined from the data using side-band techniques. In D0, the MJ background contributions passing the preselection criteria in each sample are determined from the data using an unbinned matrix method approach [41]. The "physics" backgrounds with similar event topologies are modeled using Monte Carlo event generators. The SM predictions are used to set the relative normalizations of all of the generated samples, however normalization factors are applied to samples of W bosons + n partons generated using the `ALPGEN` Monte Carlo event generator. These factors are determined at the preselection stage where the SM Higgs contribution is negligible. The predicted backgrounds model well the data in the high statistics pre-b-tag sample, as shown in figure 5.

The CDF and D0 analyses proceed by subdividing the selected sample into orthogonal subsamples based on whether either one or two jets in the event are consistent with having been initiated by a heavy b-quark, with different level ("loose (L)" or "tight (T)") of confidence. CDF has 5 tagging categories (TT,TL,LL,T,L) for the 2 jet sample, and 2 categories (TT,TL) for the 3 jet sample, while D0 uses (TT,TL,LL,T) and (LL,T) respectively. In two b-tagged jet events, the dominant remaining backgrounds are from $Wb\bar{b}$, $t\bar{t}$, and single top quark. In single b-tagged jet events the dominant backgrounds are $W+$ light or c-quark jets as well as MJ background events. To further discriminate the remaining backgrounds from the signal, MVA techniques are applied to each subsample. As an example, some of the discriminant variables used in these analyses are given in Table I.

RF Input Variable	Description
$\not\!\!E_T$	Missing transverse energy
M_W^T	Lepton-$\not\!\!E_T$ transverse mass
$p_T(\ell$-$\not\!\!E_T$ system)	p_T of W candidate
$p_T(j_1)$ ($p_T(j_2)$)	Leading (Sub-leading) jet p_T
m_{jj}	Dijet invariant mass
p_T(dijet system)	p_T of dijet system
$\Delta\mathcal{R}(j_1,j_2)$	$\Delta\mathcal{R}$ between jets
$\Delta\phi(j_1,j_2)$	$\Delta\phi$ between jets
H_T	Scalar sum of p_T of all jets

TABLE I: Description of some characteristic kinematic input quantities of the MVA technique used in the WH analyses.

Systematic uncertainties affect not only the normalization of the signal and backgrounds, but also the shape of the MVA output distributions. The influence of each source of systematic uncertainty is studied separately for each of the independent subsamples. Uncertainties in the efficiencies of selection, on jet calibration and on the b-tagging criteria affect the precision at which the background modeling is known. The uncertainties on the parton density functions, and the effect of renormalization and factorization scales on signal and background simulation are also taken into account. All these uncertainties are allowed to affect the shape of the MVA output distributions.

C. $ZH \to llb\bar{b}$

The search by the CDF and D0 collaborations at the Tevatron for the process $q\bar{q} \to ZH + X$ in which a quark-antiquark pair leads to the production of the Higgs in association with a Z boson decaying to a pair of charged lepton is also based on a total integrated luminosity $\mathcal{L} \simeq 10$ fb^{-1} [45–48]. Candidate Z boson events are preselected via their decays into e^+e^- or $\mu^+\mu^-$ pairs, and the associated Higgs boson is searched through its decay into a pair of heavy b-quarks ($H \to b\bar{b}$). At least one of the 2 or 3 jets allowed is required to be identified as a b-jet.

In this final state, which requires two leptons, the MJ background is negligible.The "physics" backgrounds are taken into account using the same Monte Carlo event generators as those used in the WH analysis.

To maximize the lepton acceptance and benefit from it, the events are classified according to the lepton types. Those having both leptons identified with high confidence (central "tight" electrons or muons) are treated separately from the others which contain “loose”, forward, or track-based leptons). These samples are analyzed independently, hence allowing for an optimal sensitivity of the sample. In addition, multivariate lepton selection are applied. To enhance the discriminating power of the jet energies and associated quantities, a neural network (NN) derived correction is applied to the jets, in CDF. This correction depends on the missing transverse energy and its orientation with respect to the jets. In D0, jet energy resolution improvements are obtained through a kinematic fit of the complete event, since all particles can be detected in this process.

These analyses also proceed by subdividing the selected sample into orthogonal subsamples based on the number and the quality of the b-tagged jets in the event CDF has four tagging categories (TT,TL,LL,T) for both the $W+2$ and $W+3$ jet samples, while D0 has a different treatment (TL,T) for the $W+3$ jet sample. Before using b-tagging, CDF employs two NNs to simultaneously separate signal events from the dominant Z+jets and kinematically different $t\bar{t}$ backgrounds. These NNs use various kinematic distributions, matrix element probabilities and the output of a separate jet flavor separating NN as inputs. In single and double b-tagged jet events, the dominant remaining background is $Zb\bar{b}$. To suppress the remaining background MVA techniques are applied to each subsample. Systematic uncertainties are overall less important than for WH since no missing transverse energy is involved, but most of the other systematic uncertainties are of similar magnitude than those of the WH analyses.

D. $ZH \to \nu\nu b\bar{b}/VH \to \not{E}_T b\bar{b}$

The remaining $b\bar{b}$ analysis is built to detect the $ZH \to \nu\nu b\bar{b}$ process, but is also sensitive to WH events in which the charged lepton is not identified, hence its more generic name $VH \to \not{E}_T b\bar{b}$. This search is also based on a total integrated luminosity $\mathcal{L} \simeq 10$ fb^{-1} [49–52]. Since in this final state there is no lepton, the event triggering and its modeling is a major difficultly. Both CDF and D0 use triggers based on $\not{E}_T$, with or without accompanying jets. The analyses are performed while studying in parallel several control samples to monitor the understanding of the background. Events are required to have significant $\not{E}_T$ and two or three jets, well separated from the $\not{E}_T$ direction. For the preselection, multivariate approaches are also applied to the events to remove a large part of the MJ background. For the final selection, b-tagging

For this analysis, the preselection plays a crucial role, given the size of the MJ background. As an example, at D0, the preselection uses the following main requirements. The events must have a well reconstructed interaction vertex and two or three jets with associated tracks to ensure efficient operation of the b-tagging algorithm. These jets must have $p_T > 20$ GeV and $|\eta| < 2.5$ and not be back-to-back in the transverse plane. $\not{E}_T$ must be greater than 40 GeV, with a significance S greater than 5 (Larger values of S correspond to $\not{E}_T$ values that are less likely to be caused by fluctuations in jet energies), and the scalar sum of the two leading jets $p_T > 80$ GeV

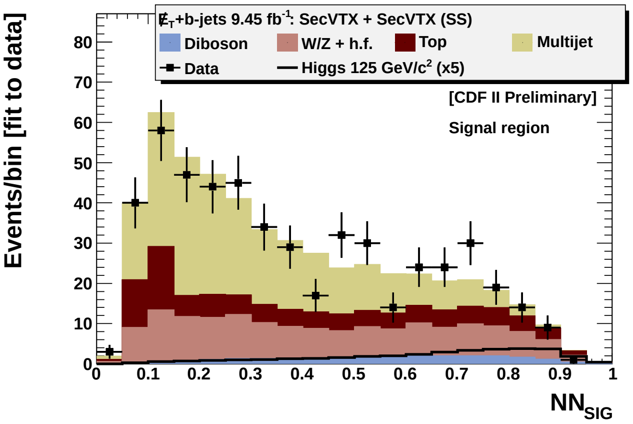

FIG. 6: Distribution of the NN discriminant in the CDF $\not{E}_T bb$ analysis for the sample with 2 b-jets tagged by two different algorithms. The data are well described by the sum of all the standard model backgrounds. The simulated signal is also represented.

The dominant signal topology is a pair of b jets recoiling against the $\not{E}_T$ due to the neutrinos from Z decay therefore with the direction of the $\not{E}_T$ at large angles to both jet directions, while in events from MJ background with fluctuations in jet energy measurement, the $\not{E}_T$ tends to be aligned with a mismeasured jet. An alternate estimate of $\not{E}_T$ can be obtained from the missing p_T calculated from the reconstructed charged particle tracks. This variable is less sensitive to jet energy measurement fluctuations and, in signal events, is also expected to point away from both jets, while in the MJ background its angular distribution is expected to be more isotropic. A variable characterizing these features is used to further reject the MJ background As for the other $b\bar{b}$ analyses, the “physics” backgrounds are taken into account using Monte Carlo event generators.

The preselected samples are subdivided into orthogonal subsamples based on the number and the quality of the b-tagged jets in the event. CDF has three tagging categories (SS,SJ,S) for analyzed 2 jet sample, where S represents a jet identified by a reconstructed secondary vertex, while J represents a jet identified by the presence of tracks not pointing to the main interaction vertex. D0 has two categories for its 2 and 3 samples (TT and LL-or-T). To suppress the remaining backgrounds multivariate discriminant technique are applied to each subsample.

E. CDF and D0 results on $H \to b\bar{b}$ searches

The results are extracted using the MVA discriminant distributions for each sub-channel of these three $H \to b\bar{b}$ analysis, and then combined. The CDF+D0 combination is discussed in section IX. Here we present the results of each collaboration, while the limits for the three different search topologies are shown in Table II. The statistical techniques used are described in section IX and allows for the extraction of the limit on the signal cross section normalized to the SM expectation, or, in case of excess, determines the p-value of the background fluctuation. At very low mass, when combining the three $H \rightarrow b\bar{b}$ topologies, CDF and D0 exclude at 95% C.L. Higgs bosons with masses smaller than 96 GeV and 102 GeV, respectively. However, in both collaboration an excess is seen in the $\simeq 120-140$ GeV range, while the expected/observed limits at $m_H = 125$ GeV are 1.8/4.2 and 2.3/3.2 times the SM expectation, for the CDF [53] and D0 [54] searches respectively. To quantify the excess, the local p-value are calculated and found to be minimal for a Higgs boson mass of 125 (135) GeV at CDF (D0), where the local significance of these deviations with respect to the background-only hypothesis is 2.7 (1.7) σ, which correspond to a 2.5 (1.5) σ global significance after applying look-elsewhere-factors (cf. section IX). These two mass values are compatible given the resolution of the dijet mass in these final states.

F. Searches with τ_h in the final state

Higgs searches using tau leptons decaying hadronically complement those using electrons and muons. CDF performs a generic analysis searching for Higgs bosons decaying to τ lepton pairs originating from direct $gg \rightarrow H$ production, associated WH or ZH production, and vector boson fusion production [55]. A final state consisting of one leptonic τ decay, one hadronic tau decay or two leptonic decays of different flavors $e\mu$ is required. CDF hadronic τ identification is performed using an MVA approach. The final discriminant for setting limits is obtained combining the output of four MVA of the signal trained against the four primary backgrounds ($Z \rightarrow \tau\tau$, $t\bar{t}$, multijet, and W+jet production). CDF also has an analysis of events that contain one or more reconstructed leptons ($\ell = e$ or μ) in addition to a τ lepton pair focusing on associated production where $H \rightarrow \tau\tau$ and additional leptons are produced in the decay of the W or Z boson [56]. Events are separated into five separate analysis channels ($\ell\ell\ell$, $e\mu\tau_h$, $\ell\ell\tau_h$, $\ell\tau_h\tau_h$, and $\ell\ell\ell\ell$). The four lepton category includes τ_h candidates. The final discriminants are likelihoods based on outputs obtained from independent MVA training against each of the primary backgrounds (Z+jets, $t\bar{t}$, and dibosons).

The D0 $\ell\tau_h jj$ analyses also include direct $gg \rightarrow H$ production, associated WH or ZH production, and vector boson fusion production [57, 58]. Decays of the Higgs boson to tau, W and Z boson pairs are considered. A final state consisting of one leptonic τ decay, one hadronic tau decay and two jets is required. Both muonic and electronic sub-channels are considered. The output of boosted decision trees is used as the final discriminant.

G. Searches for $H \rightarrow \gamma\gamma$

Both CDF [59] and D0 [60] searched for Higgs bosons decaying into diphoton pairs with the full statistics (10 fb^{-1}). The CDF analysis searches for a signal peak in the diphoton invariant mass spectrum above the smooth background originating from QCD production in several detector based categories with different signal to background ratios. In the D0 analysis the contribution of jets misidentified as photons is reduced by combining information sensitive to differences in the energy deposition from these particles in the tracker, calorimeter and central preshower in a neural network output (NNo). The output of an MVA, rather than the diphoton invariant mass, is used as the final discriminating variable. The final MVA takes as input variables the NNo, the transverse energies of the leading two photons along with the azimuthal opening angle between them, the diphoton invariant mass and transverse momentum, and additional variables, bringing an improvement in sensitivity of $\approx 20\%$.

H. Searches for $t\bar{t}H$ production

The $t\bar{t}H$ production is interesting for the direct tH coupling it involves, however its cross section is too small at the Tevatron to contribute strongly to the overall search sensitivity. CDF and D0 have studied it and given this complex final state, discrimination against the background can be achieved CDF uses several non-overlapping sets of events to search for the process $t\bar{t}H \rightarrow t\bar{t}b\bar{b}$ i) Events with a reconstructed lepton, large missing transverse energy, and four, five, and six or more jets, which are further subdivided into five b-tagging categories [61]. Neural network discriminants are used to set limits. ii) Events with no reconstructed lepton [62] are separated into two categories, one containing events with large missing transverse energy and five to nine reconstructed jets and another containing events with low missing transverse energy and seven to ten reconstructed jets. A minimum of two b-tagged jets are also required. and events with three or more b-tags are analyzed in separately from those with exactly two tags. Neural network discriminants are used to reject a part of the large MJ backgrounds and, to separate potential $t\bar{t}H$ signal events from $t\bar{t}$ background events.

V. TEVATRON HIGH MASS HIGGS SEARCHES

As the hypothesized source of electroweak symmetry breaking, the Higgs boson has strong coupling to both massive electroweak bosons. At Higgs boson masses above 135 GeV the decay to a pair of W boson is dominant, but even below the threshold to produce on shell W bosons the decay rate to one real and one virtual W boson is substantial. Both experiments pursue a strategy of searching for the $H \to W^+W^{-(*)}$ decay in final states with at least one charged lepton and from all production processes with substantial cross section. In addition searches for sub-dominant decay $H \to ZZ$ are performed. The high mass search has similar sensitivity to the individual searches for associated Higgs production with a W or Z boson performed using the $H \to bb$ decay mode at a Higgs mass of 125 GeV. As proof of principle the experiments have observed all of the direct diboson production processes with pairs of heavy gauge boson in final states that are topologically similar to those used in the Higgs search.

The primary search mode is for exclusive production via the gluon fusion process of an isolated Higgs boson with the decay, $H \to W^+W^{-(*)} \to \ell^+\nu\ell^-\bar{\nu}$, where ℓ is an electron or muon. To increase acceptance for Higgs boson production the experiments also search for gluon fusion with additional jets produced in the initial state, associated production of a Higgs boson with a massive vector boson which decays to jets, and vector boson fusion where the initial state quarks that radiate the W or Z vector bosons which fuse to a Higgs boson can be observed as jets in the final state. In addition, associated production of a Higgs boson with a massive vector boson can result in events with more than two charged leptons when the associated vector boson decays to charged leptons or events with same sign leptons when the charge of a lepton from the associated vector boson decay is the same as the charge of a lepton from the decay one of the two W bosons from the Higgs decay. In events with more than two charged leptons is is possible to search for the $H \to ZZ$ with both Z bosons decaying to charged leptons. Finally it is possible to search for $H \to W^+W^{-(*)}$ where one vector boson decays to a charged lepton and the other to quark jets. As the best production and decay modes for high mass Higgs boson searches involve one or more charged leptons maximizing the charged lepton acceptance of the detectors directly improves the sensitivity to the Higgs boson. Lepton acceptance can be improved at the trigger level on events with a charged lepton, or at the selection level by improving the efficiency for identifying charged leptons offline.

A. Diboson analysis: WW, WZ and ZZ

The diboson searches allow for testing analysis techniques and developing further understanding of the primary backgrounds to the Higgs search. The direct SM production of the WW [63, 64], WZ [65] and ZZ [66] have been observed in leptonic decays modes with two charged leptons, three changed leptons and four charged leptons respectively. The diboson searches have also been performed with larger datasets using the most modern leptons selection, providing measurements of the WW [67, 68] WZ [69, 70] and ZZ [70, 71] cross sections. In particular the published measurement of the WW cross section, $\sigma_{WW} = 12.1 \pm 0.9(\text{stat})^{+1.6}_{-1.4}(\text{syst})$ is of comparable precision to the theoretical prediction. At the Tevatron, the diboson analyses in final states with charged leptons are performed as an integral set of analyses with the high mass Higgs search. The same initial lepton based selection are used for all analysis so that techniques developed in the diboson searches can be leveraged to improve the high mass Higgs bosons search. In addition, as the direct SM diboson production processes are backgrounds to the high mass Higgs searches where the experimentally measured diboson cross sections are of similar precision to the theoretical prediction the measurements can constrain the background predictions in the Higgs search.

In addition the combined production of WW and WZ boson pairs has been observed in events with one charged lepton and jets [72] and such an approach has also been applied to perform a sensitive high mass Higgs search [73]. The combined production of all pairings of massive vector bosons has been observed in events with one vector boson decaying leptonically and the other hadronically [74].

B. Analysis Topologies

The analysis requirements typically require a lepton with $p_T > 20$ GeV, possibly additional leptons with lower thresholds, and significant $\not{E}_T$ that is not aligned along the direction of other physics objects in the events. The events are then categorized into a large number of topologies that are consistent with various Higgs boson production and decay modes. These topologies are characterized by the number of charged leptons, when there are two leptons whether the leptons are same or opposite charge, and the number of jets. Each of these topologies is analyzed separately. For these analyses, the events are generally collected using lepton based triggers. The analysis topologies and descriptions of the most significant discriminating variables follow.

i) $ggH \to W^+W^- \to \ell^+\nu\ell^-\bar{\nu} + n_j$jet [75, 76].

When $n_j = 0$, the signature is two opposite sign leptons, $\not{E}_T$, and no observed jets. The signal in this final state is almost 100% produced by the ggH process. This channel dominates the sensitivity of the high mass search. The dominant background is from SM direct WW production with minor contributions from Drell-Yan production, the WZ and ZZ diboson processes where one or more charged leptons are not detected, and W+jets or $W+\gamma$ where a jet is misidentified as a lepton or the γ converts to an electron-positron pair, only one of which is detected. The strongest discriminant is the opening angle between the leptons in 2D, $\Delta\phi$, or 3D, ΔR (figure 7), due to the spin correlation between the two spin one W bosons when decaying from the scalar Higgs boson. The collinear topology of the charged leptons also results in a low di-lepton invariant mass while Drell Yan background peaks at the Z mass and other backgrounds at large mass. The neutrinos are also collinear leading to

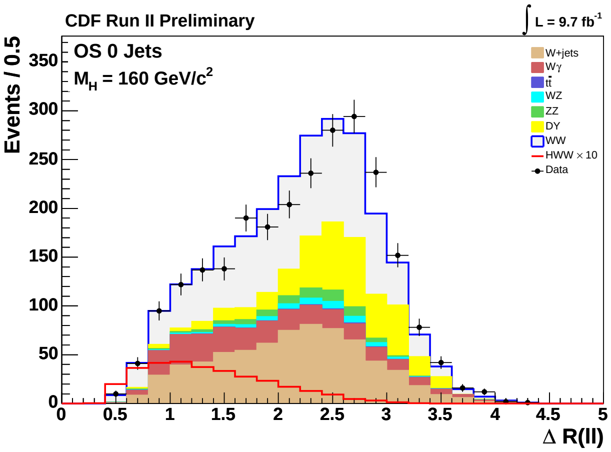

FIG. 7: The angle between the lepton candidates in three dimensions: The distribution of this angle for background and a $H \to WW$ signal with $m_h = 165$ GeV are compared

larger $\not\!\!E_T$. Matrix element based likelihood ratios are effective discriminants because in the zero jet topology the final state of either Higgs or SM direct WW production is well described by a leading order matrix element. The transverse mass of the Higgs boson can be reconstructed well since the neutrinos are also collinear. The D0 experiment further subdivides this mode by lepton flavor. CDF subdivides this analysis into modes with two well identified leptons, or one plus and an isolated track.

When $n_j = 1$, the signature is two opposite sign leptons, $\not\!\!E_T$, and one observed jet. This topology is also primarily from ggH production since the bicolored gluons or the top loop have a significant probability to radiate a high p_T gluon. This topology also has contributions from VH or VBF where one jet is observed from one of the vector boson decays or one of the final state quarks respectively. The backgrounds are the same as in the zero jet mode though top pair production with decay in the dilepton model is also a background. Drell Yan is the dominant background though there is a large contribution from SM direct WW production and W+jets is also substantial. Since ggH is still the dominant production process the effective discriminating variables are the same with the addition of H_T, the total scalar sum of energy, which is effective in reducing $t\bar{t}$ background. Finally determining whether the $\not\!\!E_T$ is aligned along the direction of a jet is also a significant discriminant since the measurement of jet energies is imprecise and can lead to falsely observed $\not\!\!E_T$.

When $n_j = 2$, the largest contribution to Higgs production is the VH process with contributions of the same order of magnitude from ggH and VBF. The dominant background is $t\bar{t}$ production in the dilepton decay mode sub-dominant contribution from Drell Yan, WW and W+jets. Since $t\bar{t}$ production is by far the dominant background an additional selection is introduced at CDF requiring that neither jet be b-tagged. Alternatively at D0 the result of a b-tagging decision is used in a final MVA discriminant. The discriminating variables are similar to the one jet analysis though variables that reject $t\bar{t}$ production such as H_T are relatively more important and variables sensitive to the dijet mass from vector boson decay in associated production and the rapidity separation of the jets in VBF are included.

ii) $VH \to VH \to VW^+W^- \to \ell^+ X \ell^+ \nu$+X [77, 78].

Associated production events can result in events with same sign leptons when the associated vector boson decays to charged leptons and the W bosons from Higgs decay with the same sign decays leptonically. The most probable decay for the remaining W boson is to quark jets. The signature of this production and decay process is two same sign leptons, $\not\!\!E_T$, and jets. The largest backgrounds are W+jets with a misidentified lepton and Drell Yan with lepton charge mismeasurement.

Associated production can also lead to trilepton events when all three vector boson decay to charged leptons. When the associated vector boson is a Z boson one of the two charged leptons is not observed. The largest background is SM direct WZ production. Variables that use the spin correlation and transverse mass of the Higgs boson are effective in this analysis. sign pairings. Associated production with a Z boson ($ZH \to ZW^+W^-$) can also lead to trilepton events when the Z boson decays to charged leptons and one of the two W bosons from the Higgs boson decay decays leptonically. These events are characterized by opposite sign same flavor lepton pair with invariant mass consistent with the Z boson mass, a third lepton, $\not\!\!E_T$, and two jets from the decay of the second W boson.

iii)$(ggH, VH, VBF) \to H \to WW \to \ell\nu + \geq 2$ jet.

Higgs can be searched inclusively in events where one of the W boson decays leptonically and the other W boson to two quark jets [79]. The dominant backgrounds are from W+jets and multijet background where a jet is misidentified as a lepton. A powerful discriminating variable unique to this mode is the reconstructed Higgs mass which can be reconstructed with a two fold ambiguity in the longitudinal momentum of the neutrino consistent with W decay.

The experiments also consider modes where one W boson decays to a τ lepton which decays hadronically [80]. Though this mode has good acceptance there is a large multijet background where jets are misidentified as τ leptons. Another mode consider events with very low dilepton invariant mass. These events have large background from two b quark production and $W\gamma$ events where the γ is radiated in the final state and is collinear. Though these modes do not have strong sensitivity they do add some sensitivity in the combination of all results. Finally a search for the Higgs boson is performed in the $H \to ZZ$ mode where both Z bosons decay to charged leptons [81]. The only significant background is this mode is SM direct ZZ production. The Higgs boson can be detected by looking for a narrow resonance in the 4 lepton invariant mass distribution. Both CDF and D0 include acceptance

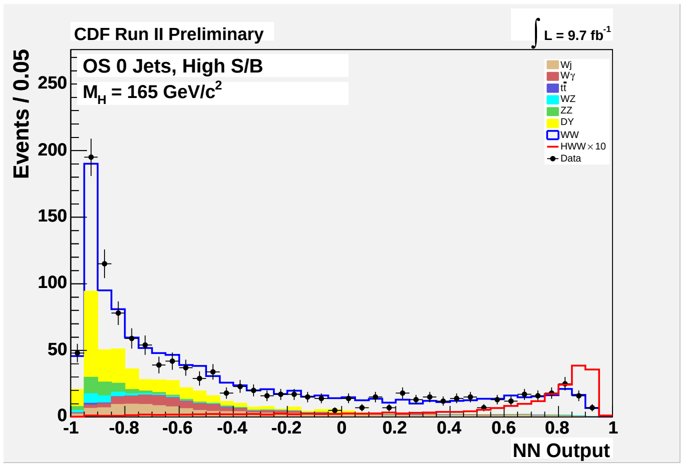

FIG. 8: NN discriminant for $ggH \to WW \to \ell\nu\ell\nu + 0$ jet at CDF. The distribution for background and a $H \to WW$ signal with $m_H = 165$ GeV (multiplied by 10) are compared.

for $H \to ZZ$ in other cases where less than four charged leptons are found in the above searches.

C. CDF and D0 results at high Higgs mass

All these search channels would select a total of approximately 75 Higgs boson events per detector if the Higgs boson mass would be 165 GeV. More than half of these events would be distinguished from the background with a good signal to background ratio using MVA discriminants as illustrated in figure 8. The comparison with the ΔR distribution (figure 7) shows that the largest discriminating power comes from this spin correlation variable, due to the unique scalar nature of the Higgs boson.

No significant excess is seen in any of the high mass Higgs search modes and limits are thus extracted, taking into account systematic uncertainties. The theory uncertainties become larger in events with more jets since, for instance, in the NNLO calculation, events with two additional jets are only calculated at NLO accuracy. These uncertainties are addressed following the treatment in [82, 83] and included in the limit extraction.

The expected limits for each experiment using the combination of all high mass Higgs search topologies at $m_H = 165$ GeV are 0.69 and 0.72 for the CDF [84] and D0 [85] searches respectively. The limits for the different search topologies are shown in Table II. The experiments each achieve expected sensitivity within a factor of approximately 1.5 of the SM cross section, in a mass range from $m_H = 140 - 185$ GeV. The CDF (D0) analysis excludes the SM Higgs boson in the mass range $m_H = 148 - 175$ GeV ($157 - 172$ GeV). Additionally the experiments provide complementary sensitivity to the production of a Higgs boson at lower masses. The expected/observed limits at $m_H = 125$ GeV are 3.1/3.0 and 3.6/4.6 for the CDF and D0 searches respectively.

VI. LHC EXPERIMENTS

A. The LHC and the ATLAS and CMS experiments

The LHC accelerator is a proton proton collider at the highest energies. During the 2011 data taking period it was configured to collide beams with 7 TeV center of mass energy and provided an integrated dataset of nearly 5 fb^{-1} to the LHC experiments while during 2012 it was configured at 8 TeV and provided integrated luminosities of 5.8(5.3) fb^{-1} to ATLAS(CMS). The instantaneous luminosity of the LHC has reached 7.7 10^{33} cm^2 s^{-1} making 20-30 multiple interactions per crossing a typical occurrence and presenting serious challenges for the experiments to trigger and reconstruct physics events. A proton proton collider at high energy provides large cross sections for gluon or quark-quark initiated Higgs production processes such as gluon fusion and vector boson fusion to a Higgs boson respectively. For instance the cross section for gluon fusion to a Higgs boson is increased by a factor of approximately 15 compared to the Tevatron case. In addition, the increase in center of mass energy from 7 to 8 TeV increased the Higgs cross section by an additional factor of approximately 30%.

The LHC experiments are forward-backward and cylindrically symmetric detectors with tracking, calorimetric and muon detection elements.

The CMS apparatus consists of a barrel assembly and two endcaps, comprising, in successive layers outwards from the collision region, a silicon pixel and strip tracker, a lead tungstate crystal electromagnetic calorimeter, a brass/scintillator hadron calorimeter, a super-conducting solenoid, gas-ionization chambers embedded in the steel return yoke for the detection of muons [86]. The silicon detector is immersed within 3.8 T magnetic solenoid and provides charged particle tracking and vertexing for b-tagging over a large pseudorapidity range of $|\eta| < 2.5$ which is well matched to the barrel and endcap electromagnetic calorimeter of muon chambers which provide coverage to $|\eta| < 3.0$ and $|\eta| < 2.4$ for electron and muon identification respectively. The return field of the magnet allows independent momentum measurement and triggering in the muon chambers. Photon and identification of τ leptons in hadronic decay modes are performed within the overlapping pseudorapidity range of the tracker and electromagnetic calorimeter. Jet finding can be performed in an expanded pseudorapidity range up to $|\eta| < 5.0$ using a forward calorimeter.

The ATLAS detector includes tracking, calorimetry and muon detection elements [87]. The inner tracking detector consists of a silicon pixel detector, a silicon micro-strip detector, and a transition radiation tracker immersed in the field of a 2 T solenoidal magnet which provides charged particle tracking and vertex finding over a large pseudorapidity range of $|\eta| < 2.5$. The inner tracker is surrounded by a high-granularity liquid-argon sampling electromagnetic calorimeter which provides electron (photon) finding in the range $|\eta| < 2.47$ ($|\eta| < 2.37$). An iron-scintillator tile calorimeter provides hadronic coverage in the central rapidity range. The endcap and forward regions are instrumented with liquid argon calorimetry for both electromagnetic and hadronic measurements which extends jet finding to $|\eta| < 4.9$. The muon spectrometer surrounds the calorimeters and consists of three large super conducting toroids, each with eight coils, a system of precision tracking chambers, and detectors for triggering in the range $|\eta| < 2.4$.

More detail about the primary systems of the experiments are given below.

1. *Tracking Detectors*

The central feature of the CMS detector is a 6 m internal diameter 3.8 T solenoidal magnet. The solenoid provides a uniform bending field for a large volume silicon strip and pixel tracker. The strip tracker consists of 10 barrel layers and 6 endcap disks at each end. The pixel detector consists of 3 barrel layers and 3 endcap disks at each end. The tracker typically allows 12 or more hits to found for all tracks including 3 layers of pixel hits and accomplishes high efficiency tracking for $|\eta| < 2.5$ as well as high efficiency primary vertex finding and b-jet identification.

The ATLAS tracker consists of a silicon pixel and strip tracker and a transition radiation straw tube tracker immersed in a 2.0 T magnetic field provided by a solenoidal magnet. The strip tracker consists of 4 barrel layers and 9 endcap disks at each end. The pixel detector consists of 2 barrel layers and 2 endcap disks at each end. The silicon inner detector tracks charged particles over the range $|\eta| < 2.5$ typically adding 3 pixels hits per tracks and allowing for high efficiency primary vertex finding and b-jet identification. The transition radiation tracker consists of 4 mm drift tubes and provides high efficiency $r-\phi$ tracking with typically 36 hits per track in the range $|\eta| < 2.0$.

2. *Calorimeters*

The CMS Calorimeter consists of a lead tungstate crystal electromagnetic calorimeter and a brass and scintillator sampling hadronic calorimeter inclosed within the solenoid. The electromagnetic calorimeter is divided into a barrel region and two endcaps which extend coverage up to $|\eta| < 3.0$. The crystals have cross sectional areas of 22x22 mm^2 in the barrel and 29x29 mm^2 in the endcap, and the calorimeter material has a Moliere radius of 21 mm leading to narrow showers and good angular resolution. The endcap calorimeter has two layers of silicon detectors interleaved with lead layers configured as a preshower detector. The excellent energy and angular resolution of the calorimeter gives a diphoton mass resolution of 1.1 GeV at a mass of 120 GeV. The hadronic sampling calorimeter is divided into a barrel region and endcaps that cover the range up to $|\eta| < 3.0$ with 7 to 11 interaction lengths of instrumented material. In addition there is a tail catcher calorimeter located outside the solenoid which increases the material of the calorimeter to at least 10 interaction lengths everywhere. An iron forward calorimeter read out by quartz fibers extends the pseudorapidity range to $|\eta| < 5.0$ to improve measurement of transverse energy and detection of missing transverse energy.

The ATLAS calorimeter uses sampling technologies over the entire angular area of coverage. The electromagnetic calorimeter is a lead-liquid argon (LAr) sampling calorimeter and is divided into overlapping barrel and endcap portions with coverage up to $|\eta| < 3.2$. The calorimeter is divided into 3 barrel and 2 endcap layers of depth with a very fine granularity in the inner layers for excellent angular resolution for electrons and photons. The barrel calorimeter has an extra inner LAr layer that functions as a preshower detector. This mass resolution for two photons at 120 GeV is approximately 1.5 GeV and the system has sufficient angular pointing ability to associate loosely photons to vertex reducing combinatoric background. The hadronic sampling calorimeter is divided into a barrel region and endcaps that cover the range up to $|\eta| < 3.2$ with 7 to 10 interaction lengths of instrumented material. The barrel region is composed of steel absorber plates with scintillating tile readout. The endcap calorimeters are based on LAr technology with copper absorber. A forward calorimeter based on copper (inner) and tungsten (outer) sampling designs extends the pseudorapidity range to $|\eta| < 5.0$. The inner copper portion give the forward calorimeter the ability to do electromagnetic calorimetry.

3. *Muons systems*

The CMS muon system makes use of three technologies interleaved in the steel return yoke of the magnet; drift tubes (central) and cathode strip chambers (forward) for precision tracking and triggering and resistive plate chambers for tracking and precision time measurement for triggering. The return field of the solenoid saturates the return yoke providing a bending field for independently measuring muon momenta. The chambers are divided into 4 stations with 14 layers of drift tubes or six layers of cathode strip chambers for robust tracking.

The ATLAS muon system is based on the magnetic deflection of muon tracks in large super-conducting air-core toroid magnets, instrumented with separate trigger and high-precision tracking chambers. The magnetic field is generated by three toroids, one in the barrel region, $|\eta| < 1.4$, and two in the endcap regions, $1.6 < \eta < 2.7$, with an overlapping region in between. This magnet configuration provides a field which is mostly orthogonal to the muon trajectories over the entire η range. Precision tracking is provided by monitored drift tubes and cathode strip chambers while resistive place chambers and thin gap chambers provide fast triggering capability based on independent measurement of the particle momentum for the central and forward regions respectively.

4. Particle flow

In CMS, jet and missing transverse energy reconstruction, and τ lepton identification are substantially improved by using particle flow identification techniques [88, 89] that classifies detector signatures as charged or neutral hadrons, photons and charged leptons using combined information from the tracker, calorimeters and muon system. Electrons, photons and neutral pions are measured in the EM calorimeter. Muons are measured in the tracker and muon system. Tau leptons in decay modes involving hadrons are found combining tracker information for charged hadrons and EM information for neutral pions. Charged hadrons in jets are measured using the tracker and neutral energy not associated to any of the above objects are measured as energy clusters in the EM and hadronic calorimeters. The vector sum of particle flow objects can also be used to identify missing transverse energy.

5. Triggering

Both detectors use a multilevel triggering system. This first level of the trigger allows reconstruction with momentum or energy measurement of physics objects including electrons and photons as electromagnetic energy deposits, muons with independent measurement of the momentum in the muons systems, jets and missing transverse energy using full calorimeter information, and taus as narrow jets. The event rate is reduced to approximately 100 kHz at level one. The ATLAS detector employs a second level trigger which repeats physics object identification using the full granularity of the detector and further reduces the event rate to 3.5kHz. Both detectors employ a full event reconstruction using optimized version of offline reconstruction code running on commercial processors as a level three or high level event filter with an output rate of about 200 Hz (ATLAS) and 500 Hz(CMS).

B. Physics object identification at the LHC

Both experiments classify observed signatures in their detectors as physics objects which can be associated to the products of high energy collision and subsequent decays. Physics analysis can be performed directly on these physics objects. The various physics signatures the experiments identify are listed below.

1. Charged Lepton Identification

Identification of electrons and muons at the LHC experiments is primarily driven by the excellent performance and hermeticity of the dedicated electron and muon identification systems and trackers.

For electron identification both experiments use clusters formed in the electromagnetic calorimeters and associate them to tracks found in the tracker by matching extrapolated position and energy [90–92]. The clustering algorithm takes into account the typical spread of the cluster in φ due to the radiation of Bremsstrahlung photons. Tracks are generally identified using inside out algorithms since the inner pixel detectors are the least occupied tracking system due to their high granularity. Electron candidates are required to pass requirements on cluster shape information, energy leakage information in the hadronic calorimeter, and track quality information. Different operating points are defined with different levels of efficiency and background rejection. Tighter operating points with lower efficiency and better background rejection include tighter criteria on identification requirements, requirements to reject electrons from photon conversions, and requirements in impact parameter to reject electrons from interactions with matter or long lived decays. The CMS experiment employs a boosted decision tree based multivariate electron identification algorithm for several analysis to improve efficiency and background rejection.

Due to the large bending fields in the muon spectrometers of the LHC experiments muons can be identified in the muon systems independently of the tracker [92–94]. In addition muons can be identified in the combined muon and tracking systems. Both experiments form combined tracker and muon system muons by associating independently reconstructed muons in the muon system to charged tracks in the tracker using position and momentum information. CMS additionally identifies muons by extrapolating tracks into the muon system to perform an inside-out search for compatible muon system hits which improved muon finding efficiency at low transverse momentums. Muons used in analysis are generally required to be identified in both systems, pass tracker hit and muon system segment requirements, and requirements on impact parameter to help reject decays to muons from long lived particles and cosmic rays.

Both experiments increase the purity of identified electrons and muons by requiring that the charged lepton candidates be isolated which rejects real and false charge leptons found in jets. The ATLAS experiment applies relative calorimeter based isolation for electrons and relative tracker based isolation for muons based on energy or tracks found in a cone around the candidate divided by the transverse energy or momentum of the candidate. The CMS experiment applied relative particle flow based isolation based on charge tracks; electromagnetic energy from electrons, photons or neutral pions; and neutral hadronic energy not associated to tracks found in a cone around the candidate and divided by the transverse energy or momentum of the candidate. These ratios are required to be less than a given value which can be adjusted to achieve different levels of performance.

The identification of hadronically decaying τ leptons is characterized by the presence of one or three charged hadrons, found as tracks with associated calorimeter energy, and possible strip shaped electromagnetic energy deposits, characteristic of neutral pion decay to photons, all located in a narrow collimated jet [95]. The ATLAS experiment combines this information together in a boosted decision tree based multivariate discriminant [96]. The CMS experiment uses a particle flow technique to measure the charged hadrons in the tracking detector and neutral pions as strips shaped electromagnetic energy deposits. It also improves the mass resolution of objects reconstructed as hadronically decaying τ by performing a fit constraining the objects from the τ decay to the τ lepton mass.

2. Photon Identification

The identification of photons uses similar criteria that that used for electrons except that events that have a track or track segment compatible with the electromagnetic cluster are rejected. Photon candidates are formed from electromagnetic clusters in the EM calorimeter [97]. The clustering algorithm and subsequent identification criteria allows for the possibility that the photon converts to an electron pair. Photon candidates are required to pass requirements on cluster shape information and energy leakage information in the hadronic calorimeter. The ATLAS experiment additionally apply isolation requirements while the CMS experiment includes the above criteria and isolation information in a boosted decision tree multivariate algorithm designed to reject non prompt sources of photons. Also the the ATLAS experiment uses the longitudinal segmentation of its EM calorimeter to require that the photons are compatible with pointing to the the primary high transverse momentum interaction vertex. In cases of conversion early in the material of the tracker both experiment reconstruct the electron position conversion pairs when possible. In this case the tracks are also required to point toward the primary interaction vertex.

3. Light and Heavy Flavor Jets

Jets are generally reconstructed using the anti-k_t algorithm based on calorimeter clusters [98]. The excellent granularity of the LHC detectors allows for the effective use of such an iterative clustering based jet finding algorithm. Raw jet energy measurements are corrected for imperfect calorimeter response using MC based corrections factors refined using studies in test beam in collision data. In high pile up conditions jets can be required to point to the hard interaction vertex. Heavy flavor jets are found based on the positive impact parameter significance of tracks and reconstructed secondary vertices [99, 100]. The ATLAS experiments combines the impact parameter significance information to form a likelihood ratio that a jet originates from a b-flavored parton or light parton. Secondary vertex information includes decay length significance and vertex mass information which is also quantified using a likelihood technique. The use of likelihood or similar techniques allows the results of the two types of algorithms to be combined into a single continuous b-flavored jet identification variable. The experiments define multiple operating points with different efficiencies and background rejection. As an example using this type of information both experiments can achieve 50% efficiency with a factor of one thousand in background rejection.

4. Missing Transverse Energy

Both experiments use measurements of missing transverse energy to identify events with neutrinos [101, 102]. The ATLAS experiment measures the visible energy using electromagnetic clusters corrected for the average hadronic component and corrected for the transverse momentum of identified muons and then infers the missing transverse energy and direction as any energy imbalance in the transverse plane. The CMS experiment uses a the particle flow method as described above to measure the visible energy and infers the $\not\!\!E_T$ in the same way. The $\not\!\!E_T$ measurement can be improved in the presence of high pile-up by associated objects used to calculate the $\not\!\!E_T$ with a given vertex. The excellent tracking efficiency and z coordinate resolution of the experiments are essential to use this technique. In addition events with false $\not\!\!E_T$ from jet mis-measurement are detected by methods such as checking whether the $\not\!\!E_T$ is collinear with jets or charged leptons or comparing with other methods of $\not\!\!E_T$ measurement such using only charged tracks in the $\not\!\!E_T$ calculation.

C. Higgs Production and Decay at the LHC

The high energy of the LHC proton-proton collider substantially increases the cross section for production of a Higgs boson via gluon fusion. The cross section for vector boson fusion and associated production are also enhanced. With larger cross section it is possible to search for inclusive Higgs production boson using fully reconstructed Higgs decays in the $H \to ZZ \to \ell^+\ell^-\nu\bar{\nu}$ and $H \to ZZ\gamma\gamma$ decay modes. Also the distinct spin correlation that leads to collinear leptons charged lepton in $H \to W^+W^{-(*)} \to \ell^+\nu\ell^-\bar{\nu}$ gives that decay mode strong sensitivity. At high Higgs mass where SM background are smaller ZZ and W^+W^- involving W and Z decays to jets or Z decays to neutrinos have strong sensitivity. Also the LHC experiments search for the Higgs boson in $H \to \tau^+\tau^-$ and in associated production with a W or Z boson with the decay $H \to bb$. The combination of these search channels gives the LHC sensitivity to search for a Higgs boson with masses from 115 GeV to order 1 TeV.

The Higgs searches at the LHC are organized by decay mode. Below we will discuss each search followed by a discussion of the results and the combination of all search results for each experiment. Previous searches at LEP, Tevatron, the LHC, and indirect constraints indicate that the Higgs boson has a low mass between approximately 115 and 130 GeV with the region around 125 GeV being of the highest interest. The LHC experiments have analyzed searches sensitive to this mass range and higher masses using datasets of approximately 5 fb^{-1} at 7 TeV and 5(CMS) 6(ATLAS) fb^{-1} at 8 TeV.

D. LHC Diboson Physics

The key modes for observing the Higgs boson at low mass are the fully reconstructed ZZ and photon-photon decay modes. To explore the role of the Higgs boson in electroweak symmetry breaking the WW decay mode is also crucial. Understanding the continuum production of these final states is important to control the background for Higgs boson searches. The LHC experiments have observed $\gamma\gamma$ production in 7 TeV pp collisions [103]. WW [104–109] and ZZ [110–113] production have been observed in both 7 and 8 TeV collisions and their cross sections measured. These searches typically used identical selection and technique to the Higgs searches. Large samples have been collected in each decay mode. With future data samples the WW and ZZ modes can be used to study the electroweak symmetry breaking related phenomena of longitudinal vector boson scattering. The contribution of Higgs exchange to this process should limit the otherwise divergent behavior of this process at high energy.

VII. LHC SEARCHES IN FERMIONIC HIGGS DECAYS

A. Searches for $t\bar{t}H$ production

The LHC experiments search for associated production of Higgs boson with $t\bar{t}$ where the Higgs boson is radiated from one of the top flavored quarks. The strong coupling between the Higgs boson and the massive top quark increased the probability of Higgs boson radiation. This process will allow the direct measurement of the top quark Yukawa coupling which is expected to be one indicating maximal coupling. Statistically it will not be as significant as measuring the coupling in gluon fusion events which are dominated by the top loop diagram, but it will not suffer from theoretical uncertainties associated with understanding the gluon fusion loop process. The ATLAS and CMS experiments have performed an analysis with the full 7 TeV data set [114, 115] in the dilepton (CMS only) and lepton plus jets decay modes of the top quarks with Higgs decay to $b\bar{b}$. Events with 4-6 (2-6) jets and 0-4 (2-4) b-tagged jets are considered at ATLAS (CMS). The ATLAS experiment uses the m_{bb} and H_T(total energy) distributions to set limits while the CMS experiment uses an MVA discriminant. The CMS experiment has sensitivity to set limits on order three to nine times the expected SM Higgs cross section with the CMS experiment achieving a sensitivity of 4.6 at a Higgs mass of 125 GeV. With a dataset of order hundreds of fb^{-1} it will be possible to directly measure the top quark Yukawa coupling in this channel.

B. Higgs searches with $H \to bb$

The LHC experiments conduct searches for associated production of Higgs boson with a W or a Z boson with subsequent decay of the Higgs boson to a pair of b quarks [116–118]. The Higgs to b quark pairs branching ratio is 70% to 40% in the Higgs boson mass range of 115-135 GeV. However, the b quark decay signature is not distinct enough to be distinguished from the background and the leptonic decay signatures of the massive vector bosons produced in associated production are necessary to search for the Higgs boson in this decay mode. These searches are organized into three sub-searches, in the same way as the Tevatron searches, by decay mode of the massive vector boson. The experiments search for $W^+H \to \ell^+\nu b\bar{b}$, $ZH \to \ell^+\ell^- b\bar{b}$, and $ZH \to \not{E}_T b\bar{b}$ where the Z decays to neutrinos. Charged leptons (ℓ) refers to electrons and muons of both electric charges. Though this set of production and decay processes is less sensitive that many of the other Higgs search modes it will be important because it can eventually be used to measure the relative couplings of the Higgs boson to the W and Z bosons and uniquely measure the coupling to the b quarks.

Data are collected on triggers that require a single charged lepton for events with W decays, single leptons (ATLAS ee mode) or pairs of leptons for Z decays to charged leptons, or either $\not{E}_T$ (ATLAS) or $\not{E}_T$+jets for events with Z decays to neutrinos.

Backgrounds such as W+jets, single top and $t\bar{t}$, dibosons and QCD multijet production with misidentified leptons are several orders of magnitude larger than the signal. To reconstruct a possible signal the analyses make the following requirements. Leptons must be fully reconstructed by both the tracking system and dedicated lepton identification systems and pass minimum transverse momentum thresholds. Missing transverse momentum must not be collinear with the jets. In addition, the ATLAS experiment requires that $\not{E}_T$ reconstructed using calorimeter and tracking methods is consistent while the CMS experiment uses particle flow based objects to take advantage of all detector subsystems. The b quarks from Higgs boson must be identified as b-jets. Finally in the $ZH \to \not{E}_T b\bar{b}$ the the $\not{E}_T$ is required to be very large. The CMS experiment selects events based on the vector boson's and Higgs candidate's transverse momenta while the ATLAS experiments separates the analysis into several bins of vector boson p_T.

CMS uses variables associated with the above quantities and the dijet invariant mass of the Higgs boson in multivariate discriminants to distinguish signal from background. The ATLAS experiment uses the invariant mass of the of the two bjets to search for Higgs boson candidates in each subset of the data and combines the results into a single search. The experiments search for a Higgs boson in the range 110-130(135 CMS) GeV using 4.7-5.0 fb^{-1} of 7 TeV collision data per experiment while the CMS experiment additionally use 5.1 fb^{-1} of 8 TeV collision data. The analysis have sensitivity to set limits on order one to five times the expected SM Higgs cross section with the CMS experiment achieving a sensitivity of 1.6 at a Higgs mass of 125 GeV. The sensitivity of this analysis will be adequate to measure the Yukawa coupling to the b quark with the order hundreds of fb^{-1} that will be collected in the post long shutdown LHC run.

C. Higgs searches with $H \to \tau^+\tau^-$

The LHC experiment search for the SM Higgs boson in the tau lepton pair decay mode [119–121]. The Higgs to τ lepton pair branching region is 8% to 1.5% in the Higgs boson mass range of 115-150 GeV and τ lepton signals are distinct enough to make this a viable search mode for all Higgs boson production processes. However, the production mode with strong sensitivity is the vector boson fusion production mode with two associated forward jets. This mode is of high interest since observation of Higgs production via vector boson fusion gives direct information on how the Higgs interacts with high energy longitudinal vector boson. In addition it will allow the measurement of the coupling of the τ lepton to the Higgs boson which is the only accessible leptonic coupling in the hadron collider environment.

The experiments search for events with zero, one or two associated jets and opposite charged τ lepton pairs with the following $\tau\tau$ decay combinations: $\ell\ell$ (ee ATLAS only), $e\tau_h$, $\mu\tau_h$ and $\tau_h\tau_h$(ATLAS) final states where τ_h indicates the τ lepton decayed to hadrons and a τ neutrino. Data are collected on triggers that require one or two charged leptons and in the ATLAS experiment two high p_T τ lepton objects ($\tau_h\tau_h$).

The primary backgrounds are Drell Yan production, W+jets production where one jet is misidentified as a τ lepton and $t\bar{t}$ production. To enhance the presence of a possible signal relative to backgrounds the leptons or sum of hadronic decay products are required to have substantial transverse energy and the $\not{E}_T$ from undetected neutrinos be collinear with the dilepton system direction. In events with two jets, the two jets are required to be high momentum and in the forward direction with a large rapidity gap consistent with the vector boson fusion hypothesis. In events with one jet, the p_T of the jet is required to be high to enhance the Higgs candidate boost, to improve the ability to distinguish Higgs signal from background and allow for the calculation of a more precise estimate of the Higgs mass.

The experiments search for the presence of a Higgs boson using methods designed to more fully reconstruct the mass of the Higgs boson by including the $\not{E}_T$ in the calculation and taking advantage of boosted configurations. The experiments search for a Higgs boson in the range 110-150 (145 for CMS) GeV using 4.7-4.9 fb^{-1} of 7 TeV collision data per experiment while the CMS experiment has additionally used 5.1 fb^{-1} of 8 TeV collision data. The ATLAS experiment reaches sensitivity to set limits in the range 3-11 times the expected SM production rate while the CMS experiment reaches sensitivities of 1.4-2.5 times the SM rate. At a mass of 125 GeV the CMS experiment sets a limit on the production cross section of a SM Higgs boson of 1.1 times the expected SM rate.

VIII. LHC SEARCHES IN BOSONIC HIGGS DECAYS

A. Higgs searches with $H \to WW, ZZ$ with decays of one boson to quarks or neutrinos

The CMS and ATLAS experiments also conduct inclusive searches for the Higgs boson in the decay modes $H \to W^+W^- \to \ell^+\nu q\bar{q}$ [122–124], $H \to ZZ \to \ell^+\ell^- q\bar{q}$ [125, 126] and $H \to ZZ \to \ell^+\ell^-\nu\bar{\nu}$ [127–129]. Through these search modes have higher backgrounds that the other decay modes to pairs of vector bosons discussed below they have strong sensitivity for high mass Higgs bosons where the vectors bosons can have high transverse momentum reducing backgrounds.

Data is collected on one and two lepton triggers for the analysis with W and Z bosons respectively. The charged leptons are required to pass transverse momentum and identification requirements. In the cases with $Z \to \ell^+\ell^-$ decays the invariant mass of the charged leptons are required to be consistent with the Z boson mass while in the $W \to \ell\nu$ case the transverse mass formed from the $\not{E}_T$ and the lepton momentum is required to be consistent with the expected W boson transverse mass. In the cases where a Z boson decays to neutrinos the $\not{E}_T$ is required to be large. The ATLAS experiment further divides this analysis into high and low mass versions where the $\not{E}_T$ is required to be larger in the high mass version. Finally in the cases where the vector bosons decay to quark the jet-jet invariant mass is required to be consistent with the expectation for a W or Z boson.

The primary backgrounds are from SM WW, WZ, and ZZ production, $t\bar{t}$ and QCD multijet production where mismeasurement of the jet fakes one of the leptonic signatures. In all of these backgrounds the diboson candidate pair is not expected to form a mass resonance or the individual vector bosons to be boosted. The experiments apply criteria to exploit these characteristics including requirements on the boost of individual vector bosons or the opening angle between vector boson decay products. After selection they search for the Higgs boson using either the full mass reconstruction ($H \to ZZ \to \ell^+\ell^- q\bar{q}$), transverses mass reconstruction $H \to ZZ \to \ell^+\ell^-\nu\bar{\nu}$ or full mass reconstruction applying a W mass constraint in the $H \to W^+W^- \to \ell^+\nu q\bar{q}$ mode. The experiments search for a Higgs boson in the range 130-600 GeV, with varying lower thresholds depending on the analysis, using 4.7-5.0 fb^{-1} of 7 TeV collision data per experiment while the CMS experiment has additionally used 5.1 fb^{-1} of 8 TeV collision data in the $H \to W^+W^- \to \ell^+\nu q\bar{q}$ and $H \to ZZ \to \ell^+\ell^-\nu\bar{\nu}$ modes. The results are substantial constraints on the mass of a high mass Higgs boson excluding masses from 230-600 GeV dominated by the $H \to ZZ \to \ell^+\ell^-\nu\bar{\nu}$ mode though extended on the lower mass edge by the $H \to W^+W^- \to \ell^+\nu q\bar{q}$ search.

B. Higgs searches with $H \to W^+W^- \to \ell^+\nu\ell^-\bar{\nu}$

The LHC experiments search for inclusive Higgs production with the decay $H \to W^+W^- \to \ell^+\nu\ell^-\bar{\nu}$ [130–133]. Both experiments have analyzed the full 2011 7 TeV dataset and 5.8 fb^{-1} (ATLAS) 5.1 fb^{-1} (CMS) 8 TeV collision data.

The decay is not fully reconstructed because of the neutrinos in the final state. However, the observation of collinear charged leptons is a distinct signature of a scalar particle decay in this mode. Observation of this signature can rule out spin 1 as a possible spin for the Higgs boson. Also, using the production rate from theory, the mode can be used to determine the Higgs boson coupling to the W boson or the ratio of the couplings to the Z boson by comparison to the $H \to ZZ$ mode. In addition, by comparing events with zero or one jet to events with two forward jets the gluon fusion and vector boson fusion production rates can be compared.

The data for the search is collected using dilepton triggers(CMS) and single lepton triggers(ATLAS). Requirements are made on the transverse momentum of the charged lepton candidates, the magnitude of the missing transverse energy and on the $\not{E}_T$ direction which must not be collinear with other physics objects in the event. Also $\not{E}_T$ measured using the calorimeter and tracker are compared to require compatibility and reject events with false $\not{E}_T$. Loose selection on the collinearity of the charged leptons is imposed to be consistent with the decay of a spin zero object to a W boson pair with subsequent leptonic decay.

CMS divides events into same flavor, electron or muon, and different flavor, electron and muon, subsamples while ATLAS only considers electron muon events as events with different flavored leptons do not have Drell Yan backgrounds and are substantially more sensitive. Both experiments divide the data into events with zero, one, or two or more jets. The primary background are SM direct diboson production, W + jets, Drell Yan and single top and $t\bar{t}$. The $t\bar{t}$ background is dominant and the division by jet counting is designed to isolate the lower jet categories which have smaller top contributions. In addition b-tag vetoes are applied including, at CMS, the vetoing of jets under the jet transverse momentum threshold. The region with b-tagged jets is used to study b-tagger performance and normalize the ttbar contribution. Events with high invariant mass dilepton mass are used to study the WW background. Both experiments have analyzed the full 2011 7 TeV dataset and 5.8 fb^{-1} (ATLAS) 5.1 fb^{-1} (CMS) 8 TeV collision data. The two experiments apply additional selection to further take advantage of the collinear nature of the charged leptons in Higgs decay to W bosons. In the two jet analysis the jets are required to have a large rapidity difference and large jet-jet invariant mass to be consistent with being forward jets from vector boson fusion.

The CMS experiment forms a boosted decision tree based multivariate descriminant to distinguish signal from background while ATLAS uses the transverse mass of the Higgs boson to search for the signal.

These analyses extend the sensitivity of the high mass searches for pairs of vector boson to lower masses including sensitivity to masses as low as 125 GeV. The experiments exclude the ranges greater than 137 GeV (ATLAS) and 129-520 GeV (CMS). No upper limit is placed in the ATLAS analysis as the analysis was optimized for low Higgs mass values. Both experiments have the sensitivity to exclude a Higgs boson at smaller masses but observe an excess around $\simeq$ 125 GeV. The ATLAS excess has a local significance of 2.8 σ and observes a signal strength of 1.4 ± 0.5 times the expected SM rate assuming a Higgs mass of 125 GeV. The CMS experiment sees a small excess with local significance of 1.6 σ.

ATLAS also conducts a search in the associated Higgs production mode with a W boson with $H \to WW$ and subsequent leptonic decays of all W boson $WH \to WW^+W^- \to \ell^+\nu\ell^+\nu\ell^-\bar{\nu}$ [134]. This mode has lesser sensitivity than the primary $H \to WW$ search and is not yet combined with the other ATLAS searches.

C. Higgs searches with $H \to ZZ \to \ell^+\ell^-\ell^+\ell^-$

Unique to the LHC experiments is the ability to observe the Higgs boson over a large range of masses through inclusive production and $H \to ZZ \to \ell^+\ell^-\ell^+\ell^-$ decay [135–138]. Both experiments have analyzed the full 2011 7 TeV dataset and 5.8 fb^{-1} (ATLAS) or 5.3 fb^{-1} (CMS) of 8 TeV collision data. In the CMS search the charged leptons considered at 7 TeV include the τ leptons [139]. The LHC experiments are designed with large angular charged lepton acceptance to detect this mode with adequate rate. In addition, because of the excellent momentum resolution of the experiments the Higgs boson mass can be reconstructed with sufficient precession that background rates are very low and event counts on order ten events are adequate for discovery. With the assumption of SM production rate the coupling the Z boson can be measured, and, by comparison to the WW mode, the ratio of W and Z couplings can be measured. Finally, with a sufficient number of events, the spin and parity of a possible Higgs boson can be determined solely from this mode using an angular analysis of the decay products.

Data is collected using single and dilepton (CMS) triggers. Transverse momentum requirements are made on the leptons to reduce backgrounds. Advanced techniques such as multivariate lepton identification are applied to maximize lepton finding efficiency. The CMS experiment improves mass resolution by using an algorithm designed to detect and recover the momentum of final state radiation photon radiated by leptons. ATLAS incorporates a similar technique as part of its electron momentum fit. One opposite charge same flavor pair of leptons is required to be consistent with the Z boson mass (ATLAS only). After these requirements the only significant background is direct SM ZZ production. A Higgs signal can be distinguished from the background by looking for a narrow resonance in the four lepton invariant mass distribution. For a Higgs mass of 125 GeV the CMS and ATLAS experiments expect $\simeq$ 10 events each.

The performance of the four lepton search including efficiency, four lepton mass scale and resolution is tested by both experiments by searching for the four lepton decay of the Z boson where one initial decay lepton radiates a photon which internally converts to a lepton anti-lepton pair, $Z \to 4\ell$. With looser selection on lepton transverse momentum and the dilepton masses of same flavor opposite sign pairs this mode can be detected with substantially higher statistical precision than a Higgs boson at low mass. Both experiment perform this analysis within the framework of the Higgs search analysis and observe this decay with the expected performance [136, 138, 140].

Both experiments use the four lepton invariant mass distribution to search for a Higgs boson. CMS further uses angular information based on the expected scalar spin zero and parity even nature of the Higgs boson in a matrix element likelihood analysis(MELA). Based on the searches large regions at high mass can be excluded. The ATLAS experiment excludes the regions 131-162 GeV and 170-460 GeV while the CMS experiment excludes the regions 131-162 GeV and 172-525 GeV. These are the largest exclusions from a single analysis channel failing to exclude only regions where the WW branching ratio dominates just above the on-shell WW production threshold, and at low masses.

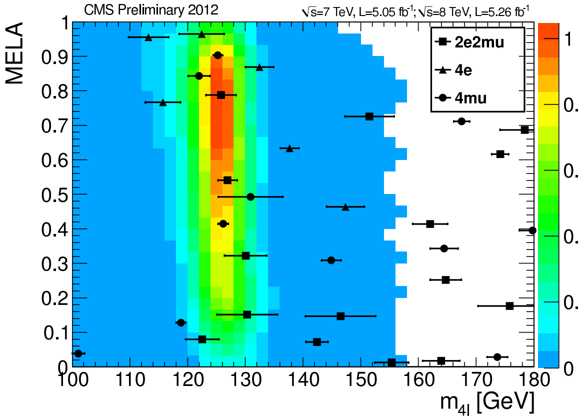

FIG. 9: A two dimensional plot of four lepton invariant invariant mass vs. matrix element likelihood from the CMS experiment. Data is shown with event by event mass uncertainties while the expectation of a 125 GeV SM Higgs boson is superimposed as a temperature plot.

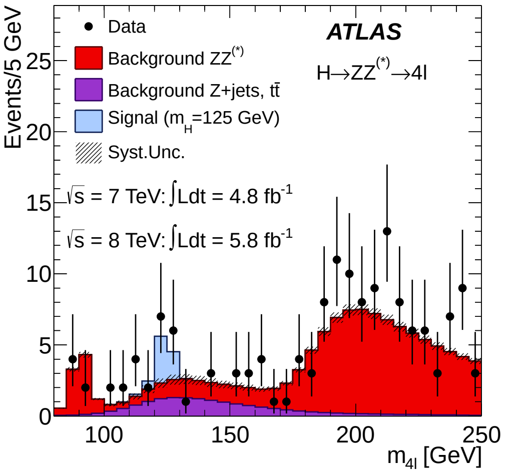

FIG. 10: The four lepton invariant mass invariant mass distribution from the ATLAS experiment. The data is displayed as point and the background expectation as a histogram. Several example SM Higgs signal are included for different hypothetical Higgs boson masses.

These analyses have strong sensitivity to Higgs boson production of a low mass Higgs of around 125 GeV, as can be seen from the invariant mass distributions of the 4 leptons candidates originating from a Z pair vs. the MELA discriminant as shown in figure 9 from CMS and the simple 4 lepton mass distribution from ATLAS is shown in figure 10. In that region both experiments see a significant excess of events. The ATLAS experiments sees a 3.4 sigma excess of events compatible with a narrow resonance of mass 125 GeV and a signal strength of 1.3 times the SM expectation. The CMS experiments sees a 3.2 sigma excess of events compatible with a narrow resonance of mass 125.6 GeV and a signal strength of approximately 0.7 times the SM expectation. The evidence presented by both experiments of a narrow resonance with decays to ZZ indicates that a new boson has been observed and the use of angular information to enhance the signal in the CMS case favors spin zero and parity even as quantum numbers for the new boson though no definitive measurement of these properties is yet possible. Further characterization of this excess is given below.

D. Higgs searches with $H \to \gamma\gamma$

The LHC experiments also have the ability to fully reconstruct a Higgs boson in the two photon decay mode [141–144]. The detectors are designed with the excellent electromagnetic energy and angular resolution necessary to accurately reconstruct the mass of two photon events. Excellent mass resolution is critical since background from multijet and multijet+photon events are large. This decay has a small branching ratio, since the Higgs can only decay to photons through a loop diagram involving massive charged particles. The large inclusive production cross section at lower masses make this a viable mode for a Higgs observation at low mass. In addition, observation of this mode would rule out spin 1 for the observed object.

Data is collected with di-photon triggers. Energy and isolation requirements are made on the photons to reduce backgrounds. Converted photons are also used and provide better energy and angular resolution when electron pairs can be reconstructed by the trackers. The ATLAS experiment reduces background by using the longitudinal segmentation of the calorimeters to select photons that point to the hard interaction vertex. Both experiments further apply a selection in events with two jets to require a vector boson fusion like topology which has good sensitivity. In the ATLAS experiment to optimize sensitivity events are divided by whether photons are converted or unconverted, by pseudorapidity region of the calorimeter they are detected in where there are resolution differences, transverse momentum of the diphoton system, and whether event pass the vector boson fusion selection since these categories have different resolution and signal to background. In the CMS experiment information from a photon identification BDT, the transverse momentums of the photons, the opening angle between the photons, the pseudo-rapidites of the photons, and the estimated resolution of the diphoton system are used to classify events by expected signal to background using a BDT multivariate discriminate. These differences in sensitivity are taken into account when calculating the sensitivity of the analysis and when determining exclusion or signal significance's. The collaborations weight events by signal to background when displaying the diphoton mass distribution to give a visual representation of the benefit of this technique.

Using the two photon invariant mass distribution to search for a Higgs boson regions at low mass and higher mass have been excluded by both experiments leaving only a narrow region of mass unexcluded. The ATLAS experiment excludes the regions 112-122.5 GeV and 132-143 GeV. This exclusion extends the lower exclusion LHC searches to the LEP excluded region and when combined with other searches excludes the entire region of masses below 600 except for the narrow allowed region around 125 GeV.

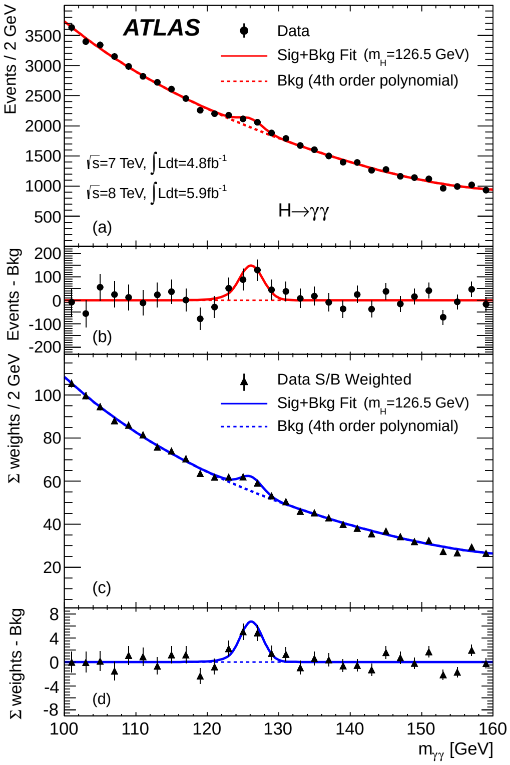

FIG. 11: Invariant mass of the diphoton events in the ATLAS experiment. The results are presented with and without event weighting by expected signal to background.

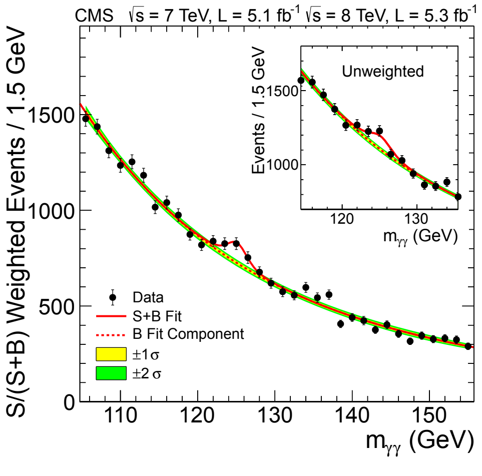

FIG. 12: Invariant mass of the diphoton events in the CMS experiment with events weighted by expected signal to background and the unweighted distribution shown as an inset.

These analyses have strong sensitivity to Higgs boson production of a low mass Higgs of around 125 GeV with expectation of observing approximately 200 events per experiment at that mass. In that region both experiments see a significant excess of events. The CMS diphoton invariant mass distribution weighted by signal to background is shown in figure 12 with the unweighted distribution inset while the corresponding ATLAS distribution are shown in in figure 11. The ATLAS experiments sees a 4.5σ excess of events compatible with a narrow resonance of mass 126.5 GeV and a signal strength of 1.9 ± 0.5 times the SM expectation. The CMS experiments sees a 4.1σ excess of events compatible with a narrow resonance of mass 125 GeV and a signal strength of 1.6 ± 0.4 times the SM expectation. The strong evidence seen by both experiments in this single mode indicates that a new boson has been observed and strongly disfavors spin one as a possible spin value. Further characterization of this excess is given below.

IX. TEVATRON, ATLAS, AND CMS RESULTS

A. Limits and Combination methods

At the LHC and at the Tevatron limits are calculated using the modified Frequentist CL_s approach. At the Tevatron, a Bayesian technique is also used. Both techniques give similar results within 5%. To ease combination of different processses, limits are obtained in units of the predicted Standard Model cross sections. The procedures are repeated at each discrete value of the generated hypothetical Higgs mass. Expected limits are calculated for both the background only hypothesis (B) for which only standard model background contributions are present in the selected data samples, and also for the signal-plus-background (S+B) hypothesis. The signal-plus-background hypothesis is calculated by including in addition the simulated signal contribution in the limit setting procedure. The limits are determined using the MVA output distributions, together with their associated uncertainties, as discriminating inputs to the limit setting procedure.

In the CL_s approach, each hypothesis is tested by repeatedly simulating the outcome of multiple pseudo-experiments. The data are assumed to be drawn from a Poisson statistical parent distribution and each pseudo experiment result is obtained by randomly generating pseudo-data using a Poisson distribution for which the mean is either taken from the background only or signal plus background hypothesis. To evaluate the statistical significance of each result a negative Poisson log likelihood ratio (LLR) test statistic is evaluated, and the outcomes are ordered in terms of their contributing statistical significance. The frequency of each outcome is used to define the shape of the resulting LLR distributions at each mass point for both the background only and signal-plus-background hypotheses.

Systematic uncertainties in each hypothesis are accounted for by nuisance parameters which are assigned a prior probability distribution. These parameters refer to uncertainties in the expected background contributions and, in the case of the signal plus background hypothesis uncertainties, also the simulated signal contribution. The nuisance parameters are Gaussian and randomly assigned within the parent distribution for each pseudo experiment. Correlations between the uncertainties are taken into account. To minimize the impact of the nuisance parameters the profile likelihood distribution is maximized over the nuisance parameters within each pseudo experiment, once for the background only and once for the signal-plus-background hypotheses. Each background is allowed to vary within its uncertainties by varying the nuisance parameters in the fitting procedure while the fit is constrained to lie within the uncertainties.

The expected limits are calculated with respect to the median of the background-only LLR distribution whereas the observed limits are quoted with respect to the single LLR value of the actual measurement. The distribution of expected limits can also be analyzed to understand the one and two σ deviations from median.

This framework can also produce statistical results quantifying expectation for and properties of a signal. Given the SM expectation for the cross section of a signal the expected p-value or probability for background only to fluctuate to the statistical significance of the expected signal can be computed. Similarly, given an excess in the observed data, the observed p-value can be computed. Finally, in this technique the SM Higgs signal cross section is multiplied by an arbitrary factor that is fit for in the likelihood minimization allowing the measurement of the observed cross section.

B. Tevatron combined results

To simplify the combination, the searches are separated into mutually exclusive final states, Table II summarizes for CDF and D0, the integrated luminosities, the Higgs boson mass ranges over which the searches are performed, the ratio limits achieved for $m_H = 125$ GeV, and the references to further details for each analysis.

Using the combination procedure outlined in the previous section, limits on the SM Higgs boson production $\sigma \times B(H \to X)$ in $p\bar{p}$ collisions at $\sqrt{s} = 1.96$ TeV for $100 \le m_H \le 200$ GeV are extracted. To facilitate comparisons with the standard model and to accommodate analyses with different degrees of sensitivity and acceptance for more than one signal production mechanism, the limits are divided by the SM Higgs boson production cross section, as a function of Higgs boson mass, for test masses for which both experiments have performed dedicated searches in different channels. A value of the combined limit ratio $\mathcal{R}$ which is less than or equal to one indicates that that particular Higgs boson mass is excluded at the 95% C.L.

The combinations of results of each single experiment [145, 146], as used in this Tevatron combination, yield the following ratios of 95% C.L. observed (expected)

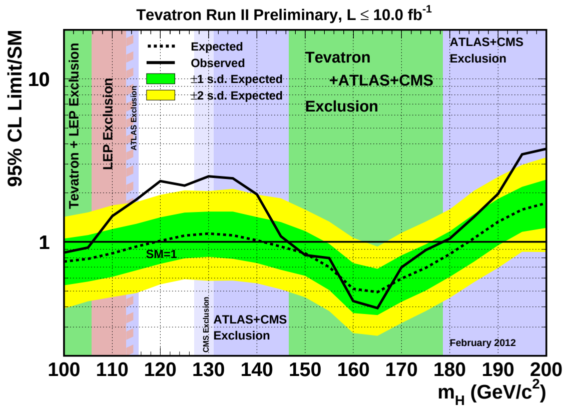

FIG. 13: Observed and expected 95% C.L. upper limits on the ratios to the SM cross section, as functions of the Higgs boson mass for the combined CDF and D0 analyses. The bands indicate the 68% and 95% probability regions where the limits can fluctuate, in the absence of signal.

limits to the SM cross section: 2.4 (1.2) for CDF and 2.2 (1.6) for D0 at $m_H = 115$ GeV, 2.9 (1.4) for CDF and 2.5 (1.9) for D0 at $m_H = 125$ GeV, and 0.42 (0.69) for CDF and 0.94 (0.76) for D0 at $m_H = 165$ GeV.

The ratios of the 95% C.L. expected and observed limit to the SM cross section are shown in figure 13 for the combined CDF and D0 analyses. The observed (expected) limit values are 1.8 (0.94) at $m_H = 115$ GeV, 2.2 (1.1) at $m_H = 125$ GeV, and 0.39 (0.49) at $m_H = 165$ GeV.

Figure 14 shows the p-value 1-CL$_\mathrm{b}$ as a function of m_H, i.e., the probability that an upward fluctuation of the background can give an outcome as signal-like as the data or more. In the absence of signal, the p-value is expected to be uniformly distributed between 0 and 1. A small p-value indicates that the data are unlikely to be explained by the background-only hypothesis, and that the data prefer the signal-plus-background prediction. The smallest observed p-value corresponds to a Higgs boson mass of 120 GeV and has a local significance of 3.0 σ. The fluctuations seen in the observed p-value as a function of the tested m_H result from excesses seen in different search channels, as well as from point-to-point fluctuations due to the separate discriminants at each m_H, as discussed in more detail below. The width of the dip from 115 to 135 GeV is consistent with the resolution of the combination of the $H \to b\bar{b}$ and $H \to W^+W^-$ channels. The effective resolution of this search comes from two independent sources. The reconstructed candidate masses, which directly constrain m_H, but also the expected cross sections times the relevant branching ratios for the $H \to b\bar{b}$ and $H \to W^+W^-$ channels which are functions of m_H in the SM. The observed excess in the $H \to b\bar{b}$ channels coupled with a less signal-like outcome in the $H \to W^+W^-$ channels determines the shape of the observed p-value as a function of m_H.

The strongest sensitivity at low mass comes from the $H \to b\bar{b}$ channels. The largest local significance in the combination of $H \to b\bar{b}$ channels is 3.3 σ at a mass of 135 GeV, while it is 2.8 σ at 125 GeV [38].

In figure 15, the fit of the signal-plus-background hypothesis to the observed data in the full mass range allows for the signal strength to vary as a function of m_H. The resulting best-fit signal strength normalized to the SM prediction is within 1 σ of the SM expectation for a Higgs boson signal in the range $110 < m_H < 140$ GeV. The largest signal fit in this range, normalized to the SM prediction, is obtained at 130 GeV, rather than at the smallest p-value mass of 120 GeV since the similar excess at these two masses translates in a higher sig-

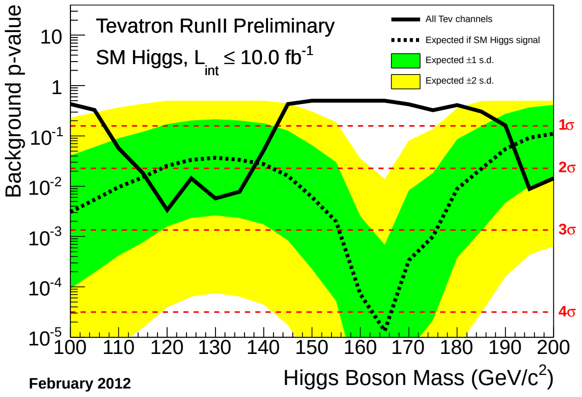

FIG. 14: The background p-values 1-CL$_\mathrm{b}$ as a function of the Higgs boson mass (in steps of 5 GeV), for the combination of the CDF and D0 analyses. The green and yellow bands correspond respectively to the regions enclosing 1 σ and 2 σ fluctuations around the median prediction in the signal-plus-background hypothesis at each value of m_H.

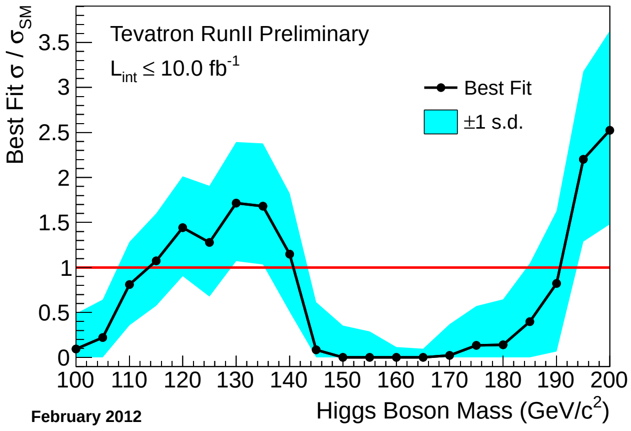

FIG. 15: The best fit signal cross section of all CDF and D0 search channels combined shown as a ratio to the standard model cross section as a function of the tested Higgs boson mass. The horizontal line at 1 represents the signal strength expected for a standard model Higgs boson hypothesis. The blue band shows the 1 σ uncertainty on the signal fit.

TABLE II: Luminosity, explored mass range, 95% C.L. expected and observed limits normalized to the SM expectation ($\mathcal{R}$) assuming $m_H = 125$ GeV, and references for the different processes and final states ($\ell = e$ or μ) for the CDF and D0 analyses.

CDF Channels	Luminosity (fb^{-1}) 2 TeV	m_H range (GeV)	exp. $\mathcal{R}$ 125 GeV	obs. $\mathcal{R}$ 125 GeV	Ref.
$WH \to \ell\nu bb$ 2-jet & 3jet channels	9.5	100−150	2.8	4.9	[43]
$ZH \to \ell^+\ell^- b\bar{b}$ 2-jet & 3 jet channels	9.5	100−150	3.6	7.2	[47]
$ZH \to \nu\bar{\nu}b\bar{b}$ 2-jet & 3jet channels	9.5	100−150	3.6	6.8	[51]
$H \to W^+W^-$ & $WH \to WW^+W^-$ & $ZH \to ZW^+W^-$	9.7	110−200	3.1	3.0	[75]
$H \to \gamma\gamma$	10.0	100−150	9.9	17.0	[59]
$H \to ZZ$ (four leptons, limits are given at 130 GeV)	9.7	120−200	18.3	20.5	[81]
$H \to W^+W^-$ ($e\tau_h$)+($\mu\tau_h$) & $WH \to WW^+W^-$ (1 τ_h)	9.7	130−200	.	.	[80]
$H + X \to \tau^+\tau^-$ (1 jet)+(2 jet)	8.3	100−150	14.8	11.7	[55]
$WH \to \ell\nu\tau^+\tau^- / ZH \to \ell^+\ell^-\tau^+\tau^-$	6.2	100−150	23.3	26.5	[56]
$WH + ZH \to jjb\bar{b}$ (SS,SJ)	9.5	100−150	9.0	11.0	[37]
$t\bar{t}H \to WWb\bar{b}b\bar{b}$ (no lepton) - (lepton)	5.7-9.5	100−150	12.4	17.6	[61, 62]

D0 Channels	Luminosity (fb^{-1}) 2 TeV	m_H range (GeV)	exp. $\mathcal{R}$ 125 GeV	obs. $\mathcal{R}$ 125 GeV	Ref.
$WH \to \ell\nu bb$ 2-jet & 3jet channels	9.7	100−150	4.7	5.2	[44]
$ZH \to \ell^+\ell^- b\bar{b}$ 2-jet & 3jet channels	9.7	100−150	5.1	7.1	[48]
$ZH \to \nu\bar{\nu}b\bar{b}$ 2-jet & 3jet channels	9.5	100−150	3.9	4.3	[52]
$H \to W^+W^- \to \ell^\pm\nu\ell^\mp\nu$	8.6-9.7	115−200	3.6	4.6	[76]
$H \to \gamma\gamma$	9.7	100−150	8.2	12.9	[60]
$H \to W^+W^- \to \mu\nu\tau_h\nu$	7.3	115−200	12.8	15.7	[57]
$H \to W^+W^- \to \ell\bar{\nu}jj$	5.4	130−200	.	.	[79]
H+X→$\ell^\pm\tau_h^\mp jj$	4.3-6.2	105−200	40.0	44.0	[57]
$VH \to \tau\tau\mu + X$	7.0	115−200	17.6	13.1	[58]
$VH \to e^\pm\mu^\pm + X$	9.7	115−200	11.6	7.8	[77]
$VH \to \ell\ell\ell + X$	9.7	100−200	11.1	19.3	[78]

nal strength at 130 GeV. The excess in signal-strenght around 200 GeV occurs in a region of low expected sensitivity, which is also expected to be contaminated by any low mass Higgs boson signal, since it would be poorly reconstructed in the $\ell\nu\ell\nu$ final states. It thus cannot be attributed to a signal at high mass.

At the Tevatron the look-elsewhere-effect (LEE) is estimated in a simplified and conservative manner. In the mass range 115–150 GeV, where the low-mass $H \to b\bar{b}$ searches dominate, the reconstructed mass resolution is approximately 15%. A LEE factor of $\simeq 2$ is thus estimated for the low-mass region. The $H \to \gamma\gamma$ searches have a much better mass resolution, of order 3%, but their contribution to the final LLR is small due to the much smaller s/b in those searches. They introduce more rapid oscillations of LLR as a function of m_H, but the magnitude of these oscillations is much smaller than those induced by the $H \to b\bar{b}$ searches. The $H \to \tau^+\tau^-$ searches have both worse reconstructed mass resolution and lower s/b than the $H \to b\bar{b}$ searches and therefore similarly do not play a significant role in the estimation of the LEE. The $H \to WW$ channel has poor mass resolution so bring only a small degradation to the LEE on the full range. For the combined search of all Tevatron channels, with a LEE of $\simeq 4$ to take into account the full range on which the search was performed, the global significance of the excess observed at low mass is approximately 2.5 σ

Applying the low mass LEE to the most significant local p-value obtained from the CDF+D0 $H \to b\bar{b}$ combination, a global significance of approximately 3.1 σ is obtained, displaying evidence for the production of a resonance in the b flavored dijet mass distribution, produced in association with a massive vector boson. Given the mass resolution in this final state, this resonance is consistent with the new boson observed by the LHC experiments, but seen for the fist time in a fermionic decay.

The measured cross section times branching ratio $\sigma_{WH} + \sigma_{ZH} \times \mathcal{B}(H \to b\bar{b})$ is shown in figure 16 as a function of m_H. and gives $= 0.23^{+0.09}_{-0.08}$ pb for $m_H = 125$ GeV, consistent with the corresponding SM prediction of 0.12 ± 0.01 pb. The best fit signal cross section of all CDF and D0 search channels split by Higgs boson decay channel is shown in figure 17, assuming $m_H = 125$ GeV.

In summary, at the Tevatron, when combining all search channels, there is significant excess of data events with respect to the background estimation in the mass range $115 < m_H < 135$ GeV. The p-value for a background fluctuation to produce such an excess corresponds to a local significance of 3.0 σ at 120 GeV. The global significance for such an excess anywhere in the full mass range is approximately 2.5 σ, after accounting for the

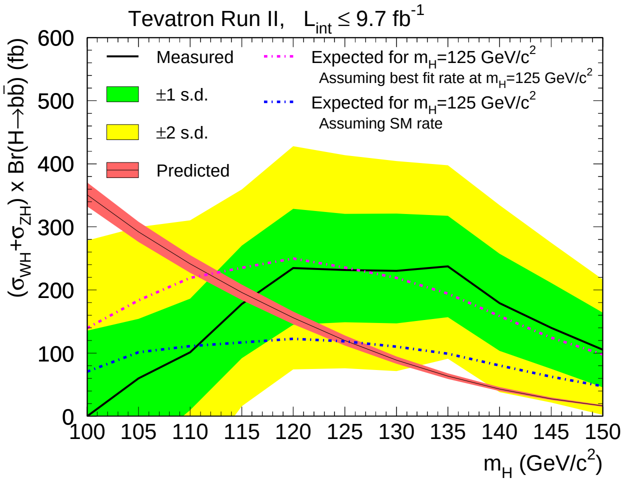

FIG. 16: The best-fit cross section times branching ratio $\sigma_{WH} + \sigma_{ZH} \times \mathcal{B}(H \to b\bar{b})$ as a function of m_H measured at the Tevatron.

look-elsewhere effect. The largest excess is observed in the $H \to b\bar{b}$ channels, corresponding to a local significance of 3.3 σ prior to accounting for the look elsewhere effect of $\simeq$2, which, when included, yields a global significance of $\approx$ 3.1 σ. Based on this result the Tevatron collaborations report evidence for the production of a resonance in the b flavored dijet mass distribution produced in association with a massive vector boson, consistent with the new boson observed by the LHC collaborations. The measured cross section for this process is consistent with the cross section expected for a SM Higgs boson of 125 GeV produced in association with a W or a Z.

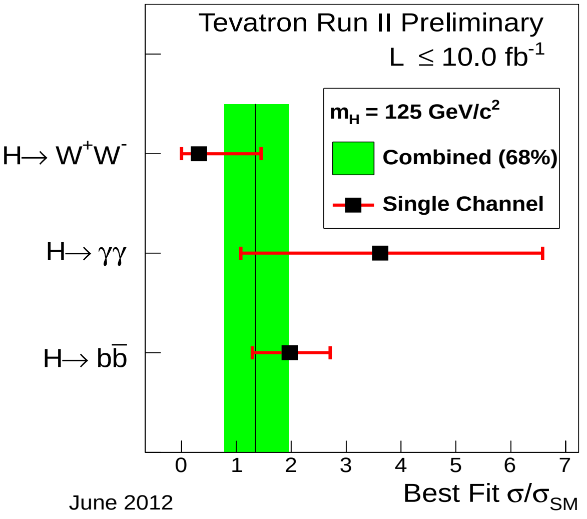

FIG. 17: SM best-fit cross sections for the three most sensitive boson decays at the Tevatron.

C. ATLAS and CMS combined results

The CMS and ATLAS experiments analyze their data using the statistical techniques described above. Each analysis channel is analyzed separately and within each experiment the Higgs results are combined [147–151]. Table III summarizes for ATLAS and CMS, the integrated luminosities, the Higgs boson mass ranges over which the searches are performed, and references to further details for each analysis. Also given are expected and observed exclusion ranges for SM Higgs boson production at 95% C.L. or when a given channel does not have sensitivity to limit the SM rate of Higgs boson production at any mass the expected and observed limit on cross section for the SM Higgs boson with mass $m_H = 125$ expressed as a multiplicative factor times the predicted SM rate. Depending on the mass of a hypothetical Higgs boson the LHC experiments have the ability to discover the Higgs boson in individual production and decay channels. At some masses it may be possible to have observations of the Higgs results in several channels. The combination of these results allow the experiments to achieve a larger exclusion range over masses where no evidence for a Higgs boson signal is seen, earlier discovery in region where several analysis channels have sensitivity, and comparison of channels to demonstrate the consistency of a possible signal with a Higgs boson hypothesis. The LHC experiment are prepared for, but have not produced a joint combination of these results. For first discovery a combination between experiments is not preferred since simultaneous observation would constitute both an observation and an independent confirmation of the result.

Over a large region of masses the LHC experiments observe no evidence for a Higgs boson. The LHC data show a consistent picture with a high mass SM Higgs typically excluded by multiple channels. At high mass the ATLAS experiment excludes the production of a SM Higgs boson with masses from 131 to 559 GeV at 95% C.L. and the CMS experiment excludes a region from 128 to 600 GeV at 95% C.L., where 600 GeV is the limit of the search range. At low mass the ATLAS experiment excludes the production of a SM Higgs boson with masses from 111 to 122 GeV at 95% C.L. and the CMS experiment excludes a region from 110 to 122.5 GeV at at 95% C.L. The combined ATLAS and CMS limits are presented in figures 18 and 19 respectively.

At low masses the experiments have the sensitivity exclude or observe the Higgs boson. The sensitivities for observation of a signal are quantified as an expected p-value for the background to fluctuate to a signal as large as the median expectation for a SM Higgs boson. The combined expected p-value at $m_H =$ 125 GeV is 4.9 σ for the ATLAS experiment and 5.8 σ for the CMS experiment. In the region around 125 GeV both experiments observe an excess of events in multiple search channels. The experiments evaluate the p-values for each channel separately

TABLE III: Luminosity, explored mass range, 95% C.L. expected and observed limits, and references for the ATLAS and CMS analyses. For analysis without SM sensitivity the expected and observed exclusion on cross section normalized to the SM expectation ($\mathcal{R}$) assuming $m_H = 125$ is given. For analysis with SM sensitivity expected and excluded ranges of mass are given.

ATLAS Channels	Luminosity (7+8 TeV, fb^{-1})	m_H range (GeV)	expected exclusion (range in GeV, $\mathcal{R}$)	observed exclusion (range in GeV, $\mathcal{R}$)	Reference
$ttH \to ttbb$	4.7	110-130	–	–	[114]
$VH \to b\bar{b}$	4.7	110-130	$\mathcal{R}$ =4.0	$\mathcal{R}$ =4.6	[116]
$H \to \tau^+\tau^-$	4.7	100-150	$\mathcal{R}$ =3.3	$\mathcal{R}$ =3.4	[119]
$H \to \gamma\gamma$	4.8+5.9	110-150	110-139.5	112-122.5 & 132-143	[141, 142]
$H \to WW \to \ell\nu\ell\nu$	4.7+5.8	110-600	>124.5	>137.0	[130, 131]
$H \to WW \to \ell\nu$2jet	4.7	300-600	–	–	[122]
$H \to ZZ \to 4\ell$	4.8+5.8	110-600	124-164 & 176-500	131-162 & 170-460	[135, 136]
$H \to ZZ \to 2\ell$2jet	4.7	200-600	351-404	300-322 & 353-410	[125]
$H \to ZZ \to 2\ell2\nu$	4.7	200-600	280-497	319-558	[127]
ATLAS Combined	4.7+5.8	110-600	110-582	111-122 & 131-559	[149]

CMS Channels	Luminosity (7+8 TeV, fb^{-1})	m_H range (GeV)	expected exclusion (range in GeV, $\mathcal{R}$)	observed exclusion (range in GeV, $\mathcal{R}$)	Reference
$ttH \to ttbb$	5.0	110-130	$\mathcal{R}$ =4.6	$\mathcal{R}$ =3.8	[115]
$VH \to b\bar{b}$	5.0+5.1	110-135	$\mathcal{R}$ =1.6	$\mathcal{R}$ =2.1	[117, 118]
$H \to \tau^+\tau^-$	4.9+5.1	110-145	$\mathcal{R}$ =1.3	$\mathcal{R}$ =1.1	[120, 121]
$H \to \gamma\gamma$	5.1+5.3	110-150	110-144	–	[143, 144]
$H \to WW \to \ell\nu\ell\nu$	4.9+5.0	120-600	122-450	129-520	[132, 133]
$H \to WW \to \ell\nu$2jet	5.0+5.1	170-600	220-515	230-480	[123, 124]
$H \to ZZ \to 4\ell$	5.1+5.3	110-600	121-570	131-162 & 172-525	[137, 138]
$H \to ZZ \to 2\ell2\tau$	4.6	190-600	–	–	[139]
$H \to ZZ \to 2\ell$2jet	4.6	130-600	–	–	[126]
$H \to ZZ \to 2\ell2\nu$	5.0+5.0	200-600	290-530	278-600	[128, 129]
CMS Combined	5.1+5.3	110-600	110-600	110-122.5 & 127-600	[151]

TABLE IV: The most significant excesses seen in ATLAS and CMS results and the combined local and global P values.

Topology	ATLAS Significance and Mass	CMS Significance and Mass
$H \to WW \to \ell\nu\ell\nu$	2.8 σ 125.0 GeV	1.6 σ 125.0 GeV
$H \to ZZ \to 4\ell$	3.4 σ 125.0 GeV	3.1 σ 125.6 GeV
$H \to \gamma\gamma$	4.5 σ 126.5 GeV	4.1 σ 125.0 GeV
Combined Significance	5.9 σ 126.0 GeV	5.0 σ 125.3 GeV

and for the entire combination and compare those values with the expected background only p-value given a SM Higgs boson as a function of mass (see figures 20,21). Information quantifying the most significant excesses in the individual search channels was given above in the sections describing the LHC Higgs searches and is summarized along with the most significant combined excess per experiment in table IV. Both experiments observe a strong Higgs boson signal with local significance's above the evidence level of 3 σ in the ZZ and $\gamma\gamma$ decay modes and combined significance's of 5.9 σ at $m_H = 126$ GeV for the ATLAS experiment and 5.0 σ at $m_H = 125.3$ for the CMS experiment. The ATLAS experiment also evaluates a global significant over their entire search range assuming to priori knowledge of the SM Higgs boson and finds a global significance of 5.1 σ. The simultaneous observation of a new particle with mass of approximately 125 GeV constitutes a definitive discovery. The decay modes in which the particle is strongly observed also confirm that the particle is a boson and plays a role in the mechanism of electroweak symmetry breaking.

The CMS and ATLAS collaborations have measured several properties to understand the compatibility of the observed boson with the SM Higgs Boson and present the results in their papers reporting the observations [149, 151]. The ATLAS collaboration reports additional properties in a companion conference note [152].

The experiments fit for the cross section for Higgs boson production given the observed data in each decay channel and globally combining all decay channels. The results are presented as a ratio to the expected SM values in figures 22 and 23 for the ATLAS and CMS experiment respectively. Of note are the larger than expected cross section times branching ratio seen in the ZZ (ATLAS) and $\gamma\gamma$ (ATLAS and CMS) decay modes. These modes have a strong contribution from

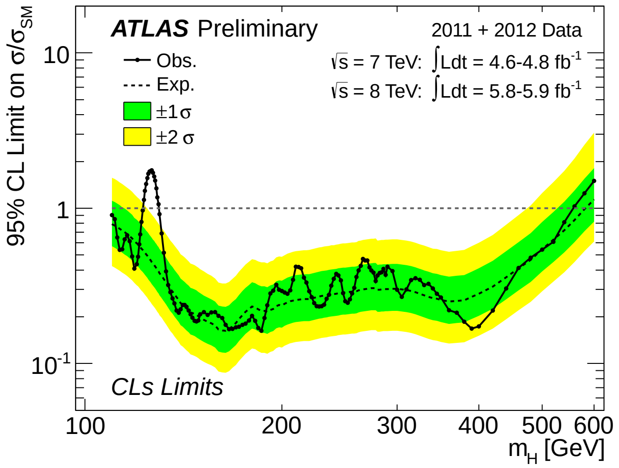

FIG. 18: The ATLAS experiments combined upper limit as a function of the Higgs boson mass between 100 and 600 GeV Solid black: observed limit/SM; Dashed black: median expected limit/SM in the background only hypothesis. Colored bands: $\pm1, 2\sigma$ distributions around median expected limit.

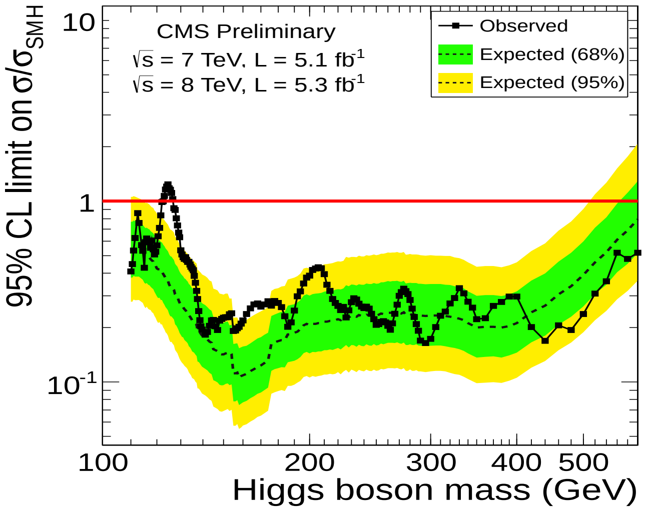

FIG. 19: The CMS experiments combined upper limit as a function of the Higgs boson mass between 100 and 600 GeV Solid black: observed limit/SM; Dashed black: CMS expected limit/SM in the background only hypothesis. Colored bands: $\pm1, 2\sigma$ distributions around median expected limit.

gluon fusion production. Also of interest is that the CMS experiment excludes a factor of 1.06 times the expected SM Higgs production cross section times BF in the $H \to \tau^+\tau^-$ decay mode at a mass 125 GeV. The ATLAS explores the coupling to the leptons in comparison to other Higgs couplings as described below. The combined signal strengths measured by the experiments are 1.4 ± 0.3 for ATLAS and 0.87 ± 0.23 for CMS compatible with the SM Higgs expectation. Individual signal strengths in the most sensitive modes are given above.

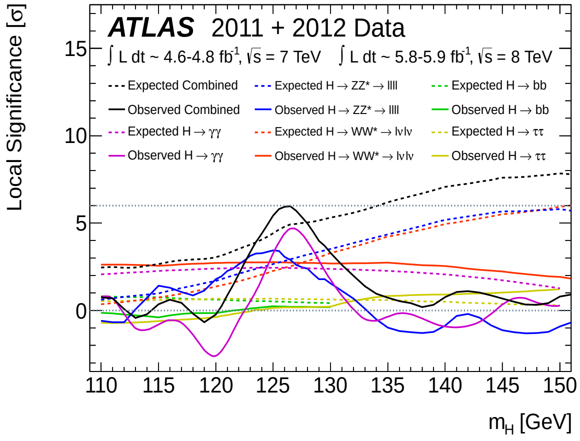

FIG. 20: ATLAS SM local p-values [149] for each search channel and the combination. The observed p-values are shown with solid curves, and the median expected p-values assuming a signal is present at the SM strength are shown with dashed curves. A dotted line indicate the 6 σ threshold.

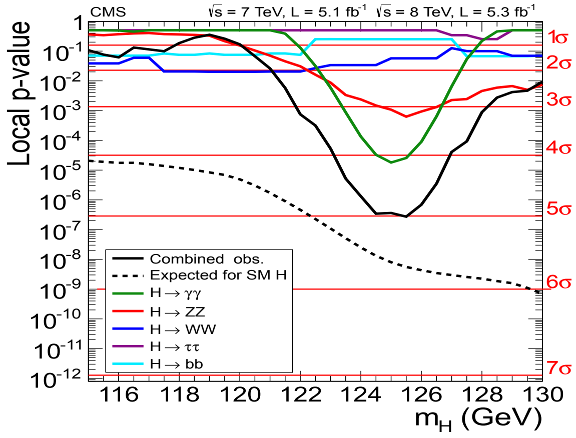

FIG. 21: CMS SM local p-values [151].The observed p-values are shown with solid curves, and the median expected p-value for the combined search assuming a signal is present at the SM strength is shown with a dashed curve. Horizontal lines indicate the $1\ \sigma - 7\ \sigma$ thresholds.

Note that the measured properties typically go as the square of the Higgs coupling constants. ATLAS converts the above number into a universal Higgs coupling constant of $K = 1.19 \pm 0.11(stat) \pm 0.03(sys) \pm 0.06(theo)$ where the experimental systematic uncertainty is separated from the theoretical uncertainties.

The CMS experiment subdivides their analysis topologies into categories sensitive to gluon fusion, vector boson fusion, associated production with a massive vector boson or associated production with a top quark and measures the production cross sections compared to the SM expectation. The results are presented in figure 24 and do not show any abnormal behavior with the current precision.

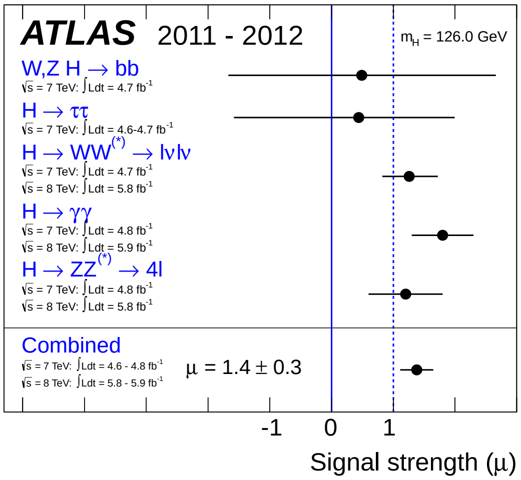

FIG. 22: ATLAS SM best-fit cross sections for all Higgs boson decays currently accessible at the LHC.

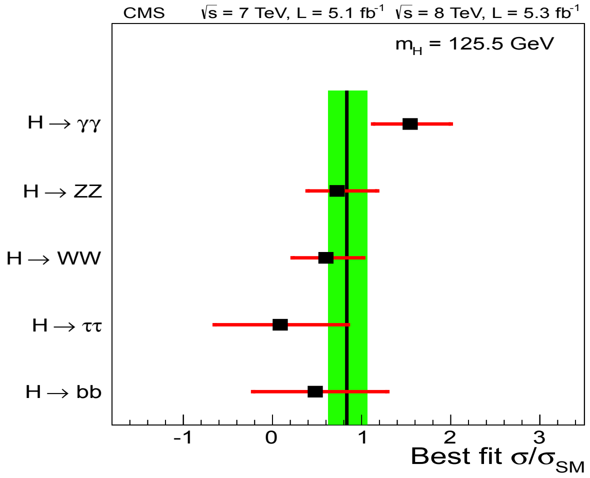

FIG. 23: CMS SM best-fit cross sections for all Higgs boson decays currently accessible at the LHC.

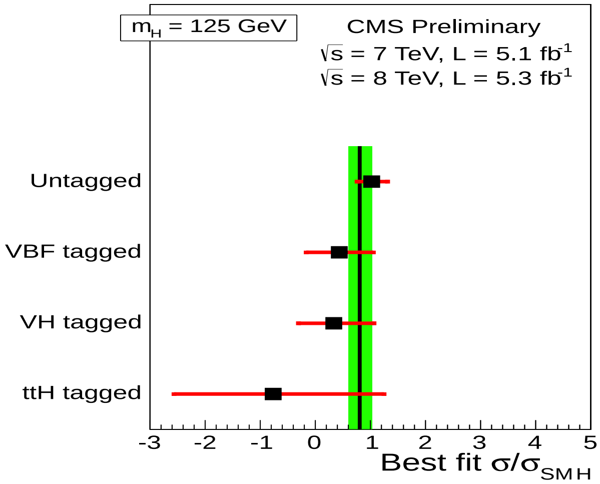

FIG. 24: CMS SM best-fit production cross sections for all Higgs production mechanisms currently accessible at the LHC. Untagged refers to the measurement for analysis topologies sensitive to gluon fusion.

The fully reconstructed decays of the Higgs boson $H \to ZZ \to \ell^+\ell^-\ell^+\ell^-$ and $H \to \gamma\gamma$ are expected to have excellent mass resolution. The $H \to W^+W^- \to \ell^+\nu\ell^-\bar{\nu}$ decay mode has substantial rate but due to the two unreconstructed neutrinos has poor mass resolution. The ATLAS experiment measures a mass for the observed boson of $m = 126.0 \pm 0.4(stat) \pm 0.4(sys)$ GeV using all three decay modes. The individual fits in a two dimensional analysis of signal strength vs. mass are shown in figure 25. The CMS experiment uses the fully reconstructed $H \to ZZ \to \ell^+\ell^-\ell^+\ell^-$ and $H \to \gamma\gamma$ modes to measure a mass of $m = 125.3 \pm 0.4(stat) \pm 0.5(sys)$ GeV. The individual and combined fits are shown in figure 26. The results are compatible with limits from previous searches and the prediction of the SM Higgs boson mass from constraints derived from Electroweak measurements.

If the observed boson is involved in the mechanism of electroweak symmetry breaking the measurement of its coupling to the W and Z bosons is a crucial discriminant. The production and decay rates measured by the experiments are compatible with the SM as shown above. The ratio of the W and Z couplings, can be computed by dividing the production times decay rates since the production of the Higgs boson takes place via the same mechanisms.The ATLAS experiment measures $R_{WZ} = 1.07^{+0.35}_{-0.27}$ and the CMS experiment measures $R_{WZ} = 0.9^{+1.1}_{-0.6}$ consistent with the SM expectation where both experiments have normalized the measurement so that the expected value in the SM is one.

The coupling of the W and Z bosons to the Higgs boson is fixed by the mechanism of electroweak symmetry breaking, while the coupling of the fermions to the Higgs boson is scaled by arbitrary Yukawa coupling constants that are related to the observed fermion masses. However, it is possible that fermionic masses do not originate from the Higgs mechanism. This can be tested by measuring the coupling of the Higgs boson to the fermions C_F, or comparing C_F and C_V, the vector boson coupling to the Higgs boson. The experiments measures these global couplings in a dimensional fit scaling the SM expectation to a value of one for each coupling as shown in figure 27. The best fit value gives $(C_V, C_F) = (1.0, 0.5)$ from the CMS experiment while the one dimensional 95% C.L. intervals when fixing the other coupling to one are [0.7:1.2] and [0.7:1.4] for C_V and [0.3,1.0] and [0.5:1.7] for C_F from the CMS and ATLAS data respectively. The data is consistent with the SM expectation at the 95% C.L. though in the case of C_F from CMS the SM value lies

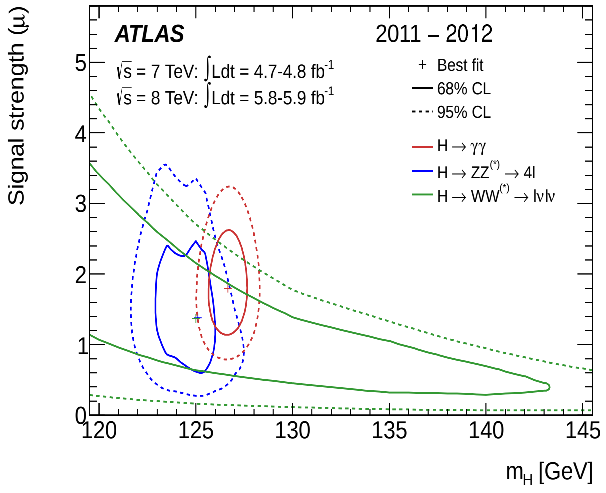

FIG. 25: The ATLAS two dimensional fit for the cross section and compared to the SM expectation and the Higgs mass for highest significance decay channels.

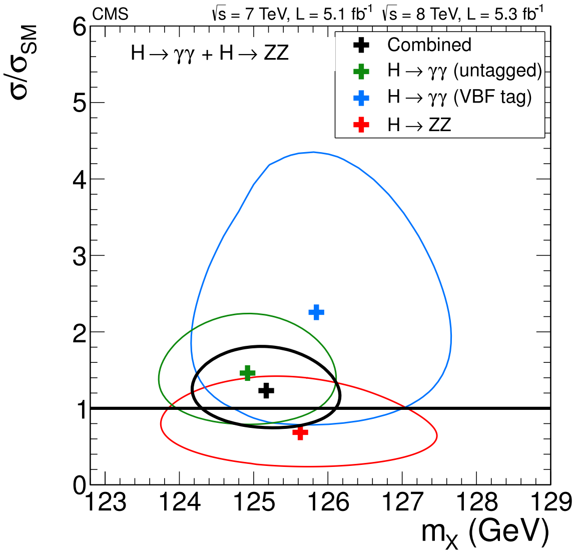

FIG. 26: The CMS two dimensional fit for the cross section and compared to the SM expectation and the Higgs mass for highest significance decay channels and the combined fit using those channels.

on the upper edge of the interval. This is related to the fermionic decay modes bb and $\tau\tau$ which show a weak signal and no signal, respectively. The ATLAS investigates the lepton couplings derived from the $H \rightarrow \tau^+\tau^-$ mode to other Higgs couplings for quarks or vector bosons. Though the lepton coupling is found to be low the result is consistent with the SM expectation at the 31% level. Further the comparison up type quark to down type quark couplings is found to be consistent with the standard model but is not constraining because of weak sensitivity.

Given the observed production and decays modes, the maximum allowed branching ratio to undetected or invisible non standard model final states can be investigated. By fixing some parameters to their SM values the ATLAS experiment places a limit of $BR < 0.84$. This branching ratio is largely unconstrained since the dominant decay mode of a 125 GeV Higgs boson have not yet been observed. Including the Tevatron data would constrain this parameter more strictly, but has not been done yet by the collaborations.

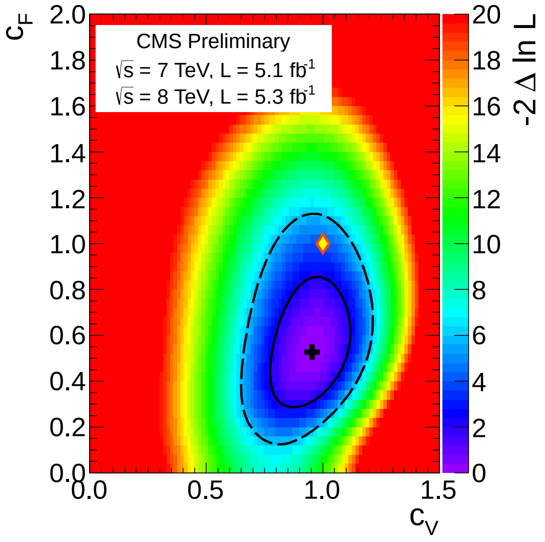

FIG. 27: The CMS two dimensional fit for global Higgs boson coupling to the vector bosons C_V on the x axis and the fermions C_F on the y axis. The $-2\Delta(ln(L))$ is indicated as a contour plot and the 68% and 95% C.L. contours are shown as solid and dashed lines respectively.

Key properties of the SM Higgs boson are the spin zero and parity even quantum numbers. The strong evidence for a new boson from two experiments in the photon-photon decay mode rules out a spin one for this boson. The near evidence from the ATLAS experiment in the WW decay mode favors spin zero. The use of angular information in the CMS evidence in the ZZ mode favors spin zero and parity even. The ZZ mode will allow a full angular analysis for spin and parity with sufficient data.

In summary, the LHC experiment have extended the LEP exclusion to 122.5 GeV and further exclude a SM Higgs boson with mass between 128 and 600 GeV. Both experiments observe a significant excess of events in the region around 125 GeV with evidence for the production of a new boson in the ZZ and $\gamma\gamma$ decay modes. Both experiments independently report the discovery of that boson and provides first measurements of its fundamental properties.

D. Conclusion and Prospects

The LHC experiments have discovered a new boson with mass around 125 GeV and have evidence for such particle in several decay modes. The Tevatron experiments report evidence for a resonance, produced in association with W and Z bosons and with decay to $b\bar{b}$, with a mass compatible to that reported by the LHC experiments. The production and decay modes that have been observed indicate that this boson plays a role in the mechanism of electroweak symmetry breaking and also in the mass generation for the quarks. The properties of this boson are compatible with those expected for a SM Higgs boson but more study is required to fully explore the nature of this discovery. The discovery of a new boson with properties indicating that it plays a role in electroweak symmetry breaking is a major significant development in fundamental physics.

The LHC experiments expect to integrate up to 30 fb^{-1} of data at 8 TeV center of mass energy this year. This data set should be sufficient to make first measurements of all accessible parameters of the boson assuming SM like behavior. After the 2012 run the LHC is expected to undergo a long shutdown to upgrade the energy and luminosity of the accelerator to near the design energy of 14 TeV and integrated luminosities per year of 100 fb^{-1}. Data taken after the upgrades should allow precision measurement of the properties of this boson and the exploration of non standard model physics associated with the boson.

---

[1] P.W. Higgs, Phys. Rev. Lett. 12, 132 (1964), *idem*, Phys. Rev. 145, 1156 (1966), F. Englert and R. Brout, Phys. Rev. Lett. 13, 321 (1964), G.S. Guralnik, C.R. Hagen, and T.W. Kibble, Phys. Rev. Lett. 13, 585 (1964)

[2] S.L. Glashow, Nucl. Phys. 20, 579 (1961), S. Weinberg, Phys. Rev. Lett. 19, 1264 (1967), A. Salam, *Elementary Particle Theory*, eds.: Svartholm, Almquist, and Wiksells, Stockholm, 1968, S. Glashow, J. Iliopoulos, and L. Maiani, Phys. Rev. D 2, 1285 (1970)

[3] J.F. Gunion, H.E. Haber, G.L. Kane, and S. Dawson, *The Higgs Hunter's Guide* (Addison-Wesley) (1990)

[4] A. Djouadi, M. Spira, P.M. Zerwas, Phys. Rev. B264, 440 (1991), S. Dawson, Nucl. Phys. B359, 283 (1991), R.V. Harlander and W.B. Kilgore, Phys. Rev. Lett. 88, 201801 (2002), C. Anastasiou, K. Melnikov, Nucl. Phys. B646, 220 (2002), V. Ravindran, J. Smith, W.L. van Neerven, Nucl. Phys. B665, 325 (2003)

[5] S. Actis, G. Passarino, C. Sturm, S. Uccirati, Phys. Lett. B670, 12 (2008), U. Aglietti, R. Bonciani, G. Degrassi, A. Vicini, Phys. Lett. B595, 432 (2004), G. Degrassi and F. Maltoni, Phys. Lett. B600, 255 (2004)

[6] C. Anastasiou, R. Boughezal and F. Petriello, JHEP 0904, 003 (2009)

[7] Kramer, Laenen and Spira, Nucl. Phys. B511, 523 (1998), Chetyrkin *et al.*, Nucl. Phys. B510, 61 (1998), S. Catani, D. de Florian, M. Grazzini, P. Nason, JHEP 0307, 028 (2003), S. Moch and A. Vogt, Phys. Lett. B631, 48 (2005), E. Laenen and L. Magnea, Phys. Lett. B632, 270 (2006), A. Idilbi, X. d. Ji, J. P. Ma, F Yuan, Phys. Rev. D 73, 077501 (2006), V. Ravindran, Nucl. Phys. B764, 291 (2006)

[8] D. de Florian and M. Grazzini, Phys. Lett. B674, 291 (2009)

[9] C. Anastasiou, S. Buehler, F. Herzog, and A. Lazopoulos, JHEP 1204 004 (2012)

[10] J. Baglio and A. Djouadi, JHEP 1103 055 (2011)

[11] D. de Florian, G. Ferrera, M. Grazzini, and D. Tommasini, JHEP 1111 064 (2011)

[12] E. Bagnaschi, G. Degrassi and A. Vicini, JHEP 1202 88 (2012)

[13] J. Beringer *et al.*, (Particle Data Group), Phys. Rev. D86, 010001 (2012)

[14] K.A.Assamagan *et al.*, arXiv:hep-ph/0406152 (2004)

[15] O. Brein, A. Djouadi, R. Harlander, Phys. Lett. B579, 149 (2004), M.L. Ciccolini, S. Dittmaier, M. Krämer, Phys. Rev. D 68, 073003 (2003), J. Baglio and A. Djouadi, J. High Energy Phys. 1010, 064 (2010), G. Ferrera, M. Grazzini and F. Tramontano, Phys. Rev. Lett. 107, 152003 (2011), A. Denner, S. Dittmaier, S. Kallweit and A. Muck, arXiv:1112.5142 [hep-ph] (2011) O. Brein, R. Harlander, M. Wiesemann and T. Zirke, arXiv:1111.0761 [hep-ph] (2011)

[16] T. Figy, S. Palmer, G. Weiglein, JHEP 1202, 105 (2012), P. Bolzoni, F. Maltoni, S.-O. Moch, M. Zaro, Phys. Rev. Lett. 105, 011801 (2010), M. Ciccolini, A. Denner, S. Dittmaier, Phys. Rev. Lett. 99, 161803 (2007), Ciccolini, A. Denner, S. Dittmaier, Phys. Rev. D 77, 103002 (2008), T. Han, G. Valencia, S. Willenbrock, Phys. Rev. Lett. 69, 3274 (1992), E.L. Berger, J. Campbell, Phys. Rev. D 70, 073011 (2004), T. Figy, C. Oleari, D. Zeppenfeld, Phys. Rev. D 68, 073005 (2003)

[17] S. Dittmaier *et. al.*, [LHC Higgs Cross Section Working Group], arXiv:1201.3084 [hep-ph] (2012)

[18] W. Beenakker, S. Dittmaier, M. Krämer, B. Plümper, M. Spira and P.M. Zerwas, Phys. Rev. Lett. 87, 201805 (2001), L. Reina and S. Dawson, Phys. Rev. Lett. 87, 201804 (2001), S. Dawson, L.H. Orr, L. Reina, D. Wackeroth, Phys. Rev. D 67, 071503 (2003), W. Beenakker, S. Dittmaier, M. Krämer, B. Plümper, M. Spira and P.M. Zerwas, Nucl. Phys. B653, 151 (2003)

[19] S. Dittmaier *et. al.*, [LHC Higgs Cross Sections Working Group], arXiv:1101.0593 [hep-ph] (2011)

[20] For a compilation of theoretical results for SM and MSSM Higgs cross sections at the LHC see: `https://twiki.cern.ch/twiki/bin/view/LHCPhysics/CrossSections`.
For the SM Higgs production via gluon fusion using Renormalization Group improved predictions see: `http://rghiggs.hepforge.org/`.

[21] LEP Electroweak Working Group, status of March 2012, `http://lepewwg.web.cern.ch/LEPEWWG/`, The ALEPH, CDF, DØ, DELPHI, L3, OPAL, SLD Collaborations, the LEP Electroweak Working Group, the Tevatron Electroweak Working Group, and the SLD Electroweak and Heavy Flavor groups, `LEPEWWG/2009-01` (2009), J. Erler and P. Langacker, *Electroweak Model*

and Constraints on New Physics, in this volume

[22] CDF and D0 Collaborations, and the Tevatron Electroweak Working Group, arXiv:1107.5255 [hep-ex] (2011)

[23] Tevatron Electroweak Working Group, CDF and D0 Collaborations, arXiv:1204.0042 [hep-ph] (2012)

[24] B.L. Ioffe and V.A. Khoze, sjNucl. Phys. 9, 50 (1978)

[25] J. Ellis *et. al.*, Nucl. Phys. B106, 292 (1976)

[26] D.R.T. Jones and S.T. Petcov, Phys. Lett. 84B, 440 (1979), R.N. Cahn and S. Dawson, Phys. Lett. 136B, 96 (1984), *ibid.*, 138B, 464 (1984), W. Kilian *et. al.*, Phys. Lett. B373, 135 (1996)

[27] ALEPH, DELPHI, L3, and OPAL Collaborations, The LEP Working Group for Higgs Boson Searches, Phys. Lett. B565, 61 (2003)

[28] CDF and D0 Collaborations, Phys. Rev. Lett. 104, 061802 (2010)

[29] GFitter collaboration, M. Baak *et al.*, Eur.Phys.J. C72 (2012) 2003

[30] CDF Collaboration, Phys. Rev. Lett. 103, 092002 (2009)

[31] D0 Collaboration, Phys. Rev. Lett.103, 092001 (2009)

[32] CDF Collaboration, J. Phys. G G 34, 2457 (2007) [hep-ex/0508029].

[33] D0 Collaboration, Nucl. Instrum. Methods, Phys. Res. A 565, 463 (2006)

[34] D0 Collaboration, Nucl. Instrum. Methods, Phys. Res. A 620, 490 (2010)

[35] CDF Collaboration, arXiv:1205.1812 [hep-ex]

[36] CDF Collaboration, Phys. Rev. D 72, 052003 (2005)

[37] CDF Collaboration, "A search for the Higgs boson in the all-hadronic channel using 9.45 fb^{-1}", CDF Conference Note 10792 (2012)

[38] CDF and D0 Collaborations, Phys. Rev. Lett. 109, 071804 (2012),

[39] CDF Collaboration, arXiv:1203.3782 [hep-ex]

[40] D0 Collaboration, arXiv:1207.6631 [hep-ex]

[41] D0 Collaboration, Phys. Rev. Lett. 102, 051803 (2009)

[42] CDF Collaboration, Phys.Rev.Lett. 103, 101802 (2009)

[43] CDF Collaboration, Phys.Rev.Lett. 109, 111804 (2012)

[44] D0 Collaboration, Phys. Rev. Lett. 109, 121804 (2012)

[45] CDF Collaboration, Phys.Lett. B715, 98 (2012)

[46] D0 Collaboration, Phys. Rev. Lett. 105, 251801 (2010)

[47] CDF Collaboration, Phys.Rev.Lett. 109, 111803 (2012)

[48] D0 Collaboration, Phys. Rev. Lett. 109, 121803 (2012)

[49] CDF Collaboration, Phys.Rev.Lett. 104, 131801 (2010)

[50] D0 Collaboration, Phys. Rev. Lett. 104, 071801 (2010)

[51] CDF Collaboration, Phys.Rev.Lett. 109, 111805 (2012)

[52] D0 Collaboration, Phys. Lett. B 716, 285 (2012)

[53] CDF Collaboration, Phys. Rev. Lett. 109, 111802 (2012)

[54] D0 Collaboration, Phys. Rev. Lett. 109, 121802 (2012)

[55] CDF Collaboration, "Search for the standard model Higgs boson in $\tau^+\tau^-$ plus jets final state with 8.3 fb^{-1} of CDF data", CDF Conference Note 10625 (2011)

[56] CDF Collaboration, "Search for the standard model Higgs in the $\ell\nu\tau\tau$ and $\ell\ell\tau\tau$ channels", CDF Conference Note 10500 (2011)

[57] D0 Collaboration, "Search for the standard model Higgs boson in tau pair final states", D0 Conference note 6305.

[58] D0 Collaboration, "Search for a standard model Higgs boson in the $\tau\tau\mu$ final state with 7.0 fb^{-1} at $\sqrt{s} = 1.96$ TeV", D0 Conference Note 6286.

[59] CDF Collaboration, "Search for a standard model Higgs boson decaying into photons at CDF using 10.0 fb^{-1} of data", CDF Conference Note 10737 (2012)

[60] D0 Collaboration, "Search for the Standard Model Higgs boson in $\gamma\gamma$ + X final states at D0 with 9.7 fb^{-1} of data", D0 Conference Note 6295.

[61] CDF Collaboration, "Search for the Higgs boson produced in association with top quarks", CDF Conference Note 10801 (2012)

[62] CDF Collaboration, "Search for standard model Higgs boson production in association with $t\bar{t}$ using no lepton final state", CDF Conference Note 10582 (2011)

[63] CDF Collaboration, Phys. Rev. Lett. 78, 4536 (1997)

[64] D0 Collaboration, Phys. Rev. Lett. 94, 151801 (2005) [Erratum-ibid. 100, 139901 (2008)]

[65] CDF Collaboration, Phys. Rev. Lett. 98, 161801 (2007)

[66] D0 Collaboration, Phys. Rev. Lett. 101, 171803 (2008)

[67] V. M. Abazov *et al.*, D0 Collaboration, Phys. Rev. Lett. 103, 191801 (2009)

[68] CDF Collaboration, Phys. Rev. Lett. 104, 201801 (2010)

[69] CDF Collaboration, Phys. Rev. D86, 031104 (2012)

[70] D0 Collaboration, Phys.Rev. D85, 112005 (2012)

[71] CDF Collaboration, Phys. Rev. Lett. 108, 101801 (2012)

[72] CDF Collaboration, Phys. Rev. Lett. 104, 101801 (2010)

[73] D0 Collaboration, Phys. Rev. Lett. 102, 161801 (2009)

[74] CDF Collaboration, Phys. Rev. Lett. 103, 091803 (2009)

[75] CDF Collaboration, "Search for $H \to WW^*$ production using 9.7 fb^{-1}", CDF Conference Note 10785 (2012)

[76] D0 Collaboration, " Search for Higgs boson production in dilepton plus missing energy final states with 8.6 - 9.7 fb^{-1} of $p\bar{p}$ collisions at $\sqrt{s} = 1.96$ TeV", D0 Conference Note 6302.

[77] D0 Collaboration, "Search for associated Higgs boson production with $VH \to e^{\pm}\nu_e\mu^{\pm}\nu_\mu + X$ like charged electron muon pairs using 9.7 fb^{-1} of $p\bar{p}$ collisions at $\sqrt{s} = 1.96$ TeV", D0 Conference Note 6301.

[78] D0 Collaboration, "Search for standard model Higgs boson with tri-leptons and missing transverse energy with 9.7 fb^{-1} of $p\bar{p}$ collisions at $\sqrt{s} = 1.96$ TeV", D0 Conference Note 6276.

[79] D0 Collaboration, "A search for the standard model Higgs boson in the $H \to WW \to \ell\nu q\bar{q}'$ Decay Channel", Phys. Rev. Lett. 106, 171802 (2011)

[80] CDF Collaboration, "Search for $H \to WW^*$ with leptons and hadronic taus in the final state using 9.7 fb^{-1}", CDF Conference Note 10781 (2012)

[81] CDF Collaboration, "An inclusive search for the Higgs boson in the four lepton final state", CDF Conference Note 10791 (2012)

[82] C. Anastasiou, G. Dissertori, M. Grazzini, F. Stockli and B. R. Webber, JHEP 0908, 099 (2009)

[83] J. M. Campbell, R. K. Ellis and C. Williams, arXiv:1005.3733 [hep-ph].

[84] CDF Collaboration, CDF Note 10804, www-cdf.fnal.gov/physics/new/hdg/Results_files/results/cdfcomb_mar2012/

[85] D0 Collaboration, D0 Note 6304-CONF, www-d0.fnal.gov/Run2Physics/WWW/results/prelim/HIGGS/H128/

[86] CMS Collaboration, *JINST* **03** (2008) S08004.

[87] ATLAS Collaboration, *JINST* **03** (2008) S08003.

[88] CMS Collaboration, CMS-PAS-PFT-09-001, http://cdsweb.cern.ch/record/1194487.

[89] CMS Collaboration, CMS-PAS-PFT-10-002, http://cms-physics.web.cern.ch/cms-physics/public/PFT-10-002-pa

[90] S. Baffioni *et al.*, Eur. Phys. J. C 49, 1099 (2007)

[91] CMS Collaboration, CMS-PAS-EGM-10-004,

http://cdsweb.cern.ch/record/1299116.
[92] ATLAS Collaboration, JHEP 1012, 060 (2010)
[93] CMS Collaboration, CMS-PAS-PFT-10-003, http://cms-physics.web.cern.ch/cms-physics/public/PFT-10-003-pas.pdf
[94] CMS Collaboration, CMS-PAS-MUO-10-002, http://cdsweb.cern.ch/record/1279140.
[95] CMS Collaboration, JINST 7 P01001 (2012),
[96] ATLAS Collaboration, ATLAS-CONF-2011-152, http://cdsweb.cern.ch/record/1398195.
[97] ATLAS Collaboration, ATL-PHYS-PUB-2011-007, http://cdsweb.cern.ch/record/1345329.
[98] M. Cacciari, G. P. Salam and G. Soyez, JHEP 0804, 063 (2008)
[99] CMS Collaboration, CMS-PAS-BTV-10-001, http://cdsweb.cern.ch/record/1279144.
[100] ATLAS Collaboration, ATLAS-CONF-2011-102, http://cdsweb.cern.ch/record/1369219.
[101] CMS Collaboration, CMS-PAS-PFT-09-001, http://cdsweb.cern.ch/record/1194487.
[102] ATLAS Collaboration, Eur. Phys. J. C 72, 1844 (2012)
[103] CMS Collaboration, JHEP 1201, 133 (2012)
[104] ATLAS Collaboration, Phys. Rev. Lett. 107, 041802 (2011)
[105] CMS Collaboration, Phys. Lett. B 699, 25 (2011)
[106] ATLAS Collaboration, Phys. Lett. B 712, 289 (2012)
[107] ATLAS Collaboration, ATLAS-CONF-2012-025, http://cdsweb.cern.ch/record/1430734.
[108] CMS Collaboration, CMS-PAS-SMP-12-005, http://cdsweb.cern.ch/record/1440234.
[109] CMS Collaboration, CMS-PAS-SMP-12-013, http://cdsweb.cern.ch/record/1460099.
[110] ATLAS Collaboration, Phys. Rev. Lett. 108, 041804 (2012)
[111] CMS Collaboration, CMS-PAS-SMP-12-007, https://twiki.cern.ch/twiki/bin/view/CMSPublic/PhysicsResultsSMP12007.
[112] ATLAS Collaboration, ATLAS-CONF-2012-090, http://cdsweb.cern.ch/record/1460409
[113] CMS Collaboration, CMS-PAS-SMP-12-014, http://cdsweb.cern.ch/record/1460100.
[114] ATLAS Collaboration, ATLAS-CONF-2012-135, http://cdsweb.cern.ch/record/1478423.
[115] CMS Collaboration, CMS-PAS-HIG-12-020, http://cdsweb.cern.ch/record/1460438.
[116] ATLAS Collaboration, Submitted to Phys. Lett. B, arXiv:1207.0210 [hep-ex].
[117] CMS Collaboration, Phys. Lett. B 710, 284 (2012)
[118] CMS Collaboration, CMS-PAS-HIG-12-019, http://cdsweb.cern.ch/record/1460692.
ATLAS-CONF-2012-015,
CONFNOTES/ATLAS-CONF-2012-015/
[119] ATLAS Collaboration, submitted to JHEP, arXiv:1206.5971 [hep-ex].
[120] CMS Collaboration, Phys. Lett. B 713, 68 (2012), arXiv:1202.4083 [hep-ex].
[121] CMS Collaboration, CMS-PAS-HIG-12-018, http://cdsweb.cern.ch/record/1460413.
[122] ATLAS Collaboration, Submitted to Phys. Lett. B, arXiv:1206.6074 [hep-ex].
ATLAS Collaboration,
[123] CMS Collaboration, CMS-HIG-12-003, https://twiki.cern.ch/twiki/bin/view/CMSPublic/Hig12003TWiki
[124] CMS Collaboration, CMS-HIG-12-021, http://cdsweb.cern.ch/record/1460660
[125] ATLAS Collaboration, Submitted to Phys. Lett. B, arXiv:1206.2443 [hep-ex].
[126] CMS Collaboration, JHEP 1204, 036 (2012)
[127] ATLAS Collaboration, Submitted to Phys. Lett. B, arXiv:1205.6744 [hep-ex].
[128] CMS Collaboration, JHEP 1203, 040 (2012)
[129] CMS Collaboration, CMS-PAS-HIG-12-023, http://cdsweb.cern.ch/record/1460693.
[130] ATLAS Collaboration, Phys. Lett. B, 716, 62 (2012),
[131] ATLAS Collaboration, ATLAS-CONF-2012-098, http://cdsweb.cern.ch/record/1462530.
CONFNOTES/ATLAS-CONF-2012-012/
ATLAS Collaboration,
[132] CMS Collaboration, CMS-PAS-HIG-12-017, http://cdsweb.cern.ch/record/1460424.
[133] CMS Collaboration, Phys. Lett. B 710, 91 (2012)
[134] ATLAS Collaboration, ATLAS-CONF-2012-078, atlas.web.cern.ch/Atlas/GROUPS/PHYSICS/CONFNOTES/ATLAS-CONF-2012-078/.
[135] ATLAS Collaboration, Phys. Lett. B 710, 383 (2012)
[136] ATLAS Collaboration, ATLAS-CONF-2012-092, http://cdsweb.cern.ch/record/1460411.
[137] CMS Collaboration, Submitted to Phys. Rev. Let. arXiv:1202.1997 [hep-ex].
[138] CMS Collaboration, CMS-PAS-HIG-12-016, http://cdsweb.cern.ch/record/1460664.
[139] CMS Collaboration, JHEP 1203, 081 (2012)
[140] CMS Collaboration, CMS-PAS-SMP-12-009, http://cdsweb.cern.ch/record/1431862.
[141] ATLAS Collaboration, Phys. Rev. Lett. 108, 111803 (2012)
[142] ATLAS Collaboration, ATLAS-CONF-2012-091, atlas.web.cern.ch/Atlas/GROUPS/PHYSICS/CONFNOTES/ATLAS-CONF-2012-091/
[143] CMS Collaboration, Phys. Lett. B 710, 403 (2012)
[144] CMS Collaboration, CMS-PAS-HIG-12-015, http://cdsweb.cern.ch/record/1460419.
[145] CDF Collaboration, “Combination of CDF standard model Higgs boson searches with up to to 9.7 fb^{-1} of data”, CDF Conference Note 10804 (2012)
[146] “Combined Upper Limits on Standard Model Higgs Boson Production from the D0 Experiment in up to 9.7 fb^{-1} of data”, D0 Conference Note 6304 (2012)
[147] ATLAS Collaboration, ATLAS-CONF-2012-019, atlas.web.cern.ch/Atlas/GROUPS/PHYSICS/CONFNOTES/ATLAS-CONF-2012-019/
[148] ATLAS Collaboration, Phys. Lett. B 710, 49 (2012)
[149] ATLAS Collaboration, Phys. Lett. B 716, 1 (2012) arXiv:1207.7214 [hep-ex].
[150] CMS Collaboration, Phys. Lett. B 710, 26 (2012)
[151] CMS Collaboration, Phys. Lett. B 716, 30 (2012) arXiv:1207.7235 [hep-ex].
[152] ATLAS Collaboration, ATLAS-CONF-2012-127, atlas.web.cern.ch/Atlas/GROUPS/PHYSICS/CONFNOTES/ATLAS-CONF-2012-127/